

1 Quantifying methane emissions from natural gas production in 2 northeastern Pennsylvania

3 Zachary R. Barkley¹, Thomas Lauvaux¹, Kenneth J. Davis¹, Aijun Deng¹, Yanni Cao¹, Natasha L.
4 Miles¹, Scott J. Richardson¹, Colm Sweeney², Anna Karion³, MacKenzie Smith⁴, Eric A. Kort⁴, Stefan
5 Schwietzke⁵, Thomas Murphy⁶, Guido Cervone⁷, Douglas Martins⁸, Joannes D. Maasakkers⁹

6 ¹Department of Meteorology, The Pennsylvania State University, University Park, PA 16802, United States

7 ²NOAA/Earth Systems Research Laboratory, University of Colorado, Boulder, CO, 80305, United States

8 ³National Institute of Standards and Technology, Gaithersburg, MD 20899, United States

9 ⁴Department of Climate and Space Sciences and Engineering, University of Michigan, Ann Arbor, MI, 48109, United States

10 ⁵Cooperative Institute for Research in Environmental Sciences, University of Colorado, Boulder, Colorado, USA.

11 ⁶Marcellus Center for Outreach and Research, The Pennsylvania State University, University Park, PA 16802, United States

12 ⁷Department of Geography, The Pennsylvania State University, University Park, PA 16802, United States

13 ⁸FLIR Systems, West Lafayette, IN 47906, United States

14 ⁹School of Engineering and Applied Sciences, Harvard University, Pierce Hall, 29 Oxford Street, Cambridge, Massachusetts
15 02138, United States

16

17

18 *Correspondence to:* Zachary R. Barkley (zrb5027@psu.edu)

19

20

21 **Abstract.** Natural gas infrastructure releases methane (CH₄), a potent greenhouse gas, into the atmosphere. The estimated
22 emission rate associated with the production and transportation of natural gas is uncertain, hindering our understanding of its
23 greenhouse footprint. This study presents a new application of inverse methodology for estimating regional emission rates
24 from natural gas production and gathering facilities in northeastern Pennsylvania. An inventory of CH₄ emissions was
25 compiled for major sources in Pennsylvania. This inventory served as input emission data for the Weather Research and
26 Forecasting model with chemistry enabled (WRF-Chem), and atmospheric CH₄ mole fraction fields were generated at 3 km
27 resolution. Simulated atmospheric CH₄ enhancements from WRF-Chem were compared to observations obtained from a
28 three-week flight campaign in May 2015. Modelled enhancements from sources not associated with upstream natural gas
29 processes were assumed constant and known and therefore removed from the optimization procedure, creating a set of
30 observed enhancements from natural gas only. Simulated emission rates from unconventional production were then adjusted
31 to minimize the mismatch between aircraft observations and model-simulated mole fractions for ten flights. To evaluate the
32 method, an aircraft mass balance calculation was performed for four flights where conditions permitted its use. Using the
33 model optimization approach, the weighted mean emission rate from unconventional natural gas production and gathering
34 facilities in northeastern Pennsylvania approach is found to be 0.36% of total gas production, with a 2 σ confidence interval
35 between 0.27-0.45% of production. Similarly, the mean emission estimates using the aircraft mass balance approach is

36 calculated to be 0.40% of regional natural gas production, with a 2σ confidence interval between 0.08-0.72% of production.
37 These emission rates as a percent of production are lower than rates found in any other basin using a top-down methodology,
38 and may be indicative of some characteristics of the basin that makes sources from the northeastern Marcellus region unique.

39 **1 Introduction**

40 The advent of hydraulic fracturing and horizontal drilling technology has opened up the potential to access vast reservoirs of
41 natural gas previously inaccessible, shifting energy trends in the United States away from coal and towards natural gas (EIA,
42 2016b). From a greenhouse gas (GHG) emissions perspective, natural gas has the potential to be a cleaner energy source
43 than coal. For every unit of energy produced, half as much carbon dioxide (CO_2) is emitted through the stationary
44 combustion of natural gas in comparison to coal (EPA, 2016). However, during the process of extracting and distributing
45 natural gas a percentage of the overall production escapes into the atmosphere through both planned releases and unintended
46 leaks in infrastructure. Though these emissions may be small from an economic perspective, their climatological impacts are
47 not negligible (Alvarez et al., 2012; Schwietzke et al., 2014). Methane (CH_4), the main component of natural gas, is a potent
48 greenhouse gas with a global warming potential over a 20-year period (GWP_{20}) of 84 (Myhre et al., 2013). Over a 100-year
49 period the GWP is reduced to 28 due mostly to interactions with the hydroxyl radical which transform the CH_4 molecule to
50 CO_2 . Depending on which timespan is used, the relative climatological impacts of natural gas as an energy source compared
51 to coal can vary. Using the GWP_{20} value, it is estimated that a natural gas emission rate of greater than 3% of total gas
52 production would result in a natural gas power plant having a more negative impact on the climate than a coal-powered
53 plant. Using the GWP_{100} value, this emission rate threshold shifts to 10% of production (Schwietzke et al., 2014; Alvarez et
54 al., 2012). Complicating matters further, the future climate impacts associated with an increased availability of natural gas
55 extends well beyond a simple greenhouse gas footprint comparison against coal. Lower fuel prices linked to this new
56 reservoir of energy can change the course of future energy development globally. With many states and countries attempting
57 to find a suitable balance between their energy policies and greenhouse gas footprint, it is important for the scientific
58 community to be able to quantify and monitor natural gas emission rates.

59 The drilling and transportation of natural gas can be broken down into five stages: production, processing, storage,
60 transmission, and distribution. The United States Environmental Protection Agency (EPA) uses a bottom-up approach to
61 quantify these emissions, estimating emission rates per facility or component (such as a compressor, unit length of pipeline,
62 pneumatic device) or an average emission per event (such as a well completion or liquids unloading). These “emission
63 factors” are then multiplied by nationwide activity data containing the number of components or events associated with each
64 emission factor, and a total emission rate is produced for the country (EPA, 2015b). This bottom-up approach is a practical
65 methodology for estimating emissions over a large scale but has limitations. A bottom-up inventory depends on the quality
66 and quantity of its emission factors and activity data. Emissions from sources in the natural gas industry can be temporally
67 variable and have a wide range of values depending on a number of factors, such as the quality and age of the device and the

68 gas pressure moving through the component. Furthermore, recent studies have shown that a majority of emissions comes
69 from a small percentage of devices, often referred to as “super-emitters”, creating a long-tail distribution of emission sources
70 (Brandt et al., 2014, Omara et al., 2016, Zavala-Araiza et al., 2015, 2017, Frankenberg et al., 2016). These factors make it
71 difficult to sample enough devices and adequately describe the mean emission rate, thus allowing for significant
72 representation errors in the emission factors. Because emission factors are required for hundreds of different components,
73 these errors can accumulate and lead to systematic biases in the total emissions estimate.

74 One way to compliment results based on inadequate sample sizes in the bottom-up approach is to measure the
75 aggregated enhancement in the atmospheric mole fraction at larger scales through a top-down approach. Instead of
76 measuring emissions from individual devices and scaling up, a top-down approach takes atmospheric greenhouse gas
77 concentrations measured downwind of a continent (e.g. Bousquet et al., 2006), a region (e.g. Lauvaux et al., 2008), a city
78 (e.g. White et al., 1976, Mays et al., 2009, Lamb et al., 2016) or a facility (e.g. Ryerson et al., 2001) and uses inverse
79 methodologies to attribute the enhancements to potential sources upwind. One of these methods, the aircraft mass balance
80 technique, has been performed at many different oil and gas fields to characterize natural gas emissions (Petron et al., 2012,
81 Karion et al., 2013, 2015, Peischl et al., 2015, Conley et al., 2016). While this methodology is able to capture surface fluxes
82 over a large region, it remains difficult to attribute the emissions to any individual source (Cambaliza et al., 2014). Any
83 sources from within the flux region that emit CH₄ will be measured in the downwind observations and be a part of the
84 aggregated regional enhancement. Atmospheric observations may include other sources of CH₄ unrelated to natural gas, such
85 as anaerobic respiration from landfills and wetlands, enteric fermentation from cattle, anaerobic decomposition of manure,
86 CH₄ seepage from coal mining, and many other smaller sources. If the purpose of the study is to solve for the emissions from
87 the natural gas industry, emissions from all sources unrelated to natural gas must be known and removed from the regional
88 flux estimate. Thus, top-down experiments require an accurate CH₄ inventory of the study area and any errors associated
89 with the inventory will propagate into the final emissions estimate. A more advanced technique to separate out non-natural
90 gas sources has been developed using ethane as a tracer for natural gas (Smith et al., 2015). However, such methods may
91 struggle in dry gas basins where smaller ethane to methane ratios within the gas can make the ethane signature more difficult
92 to separate out, or in regions where multiple ethane sources are present. And similar to bottom-up methods, top-down studies
93 fail to address temporal variability, with observations from many of these studies having been collected during a limited
94 number of 2 to 4 hour aircraft flights performed over a period of weeks.

95 In recent years, both bottom-up and top-down studies have aimed at calculating natural gas emission rates, with
96 bottom-up studies generally finding smaller emission rates than their top-down counterparts (Brandt et al., 2014). The
97 discrepancy between the results from these two methodologies must be better understood if the true emission rate is to be
98 known. Both the bottom-up and top-down approaches have their own inherent sources of error. For the bottom-up approach,
99 a small sample size could result in the omission of any super-emitters, resulting in a low emissions bias. For the top-down
100 approach, difficulty in attributing the measured enhancements to their correct sources can lead to errors when solving for the
101 emissions of a particular sector.

102 Top-down emission estimates of individual basins have shown variation in the emission rate across the different
103 basins. An aircraft mass balance performed over the Barnett shale in Texas found an emission rate between 1.3-1.9% of
104 production (Karion et al., 2015), yet a similar mass balance study executed over unconventional wells in Uintah County,
105 Utah, calculated an emission rate between 6.2-11.7% of production (Karion et al., 2013). Differences in regional emission
106 rates can perhaps best be illustrated by recent studies in the Marcellus region. The Marcellus shale gas play is part of the
107 Marcellus geological formation running close to the Appalachian mountain chain from West Virginia to southern New York
108 and contains an estimated 140 billion cubic feet of technically recoverable natural gas (EIA, 2012). Reaching peak
109 production by the end of 2015, the Marcellus is the largest producing shale in the U.S., producing 17,000 million standard
110 cubic feet per day (MMSCFD) of natural gas (EIA, 2016a). A bottom-up study measuring emissions from 17 unconventional
111 well-sites in the Marcellus found a median emission rate from the wells of 0.13% of production, but estimated a mean
112 emission rate between 0.38-0.86% of production due to the potential presence of super-emitters which would skew the mean
113 emission rate towards values higher than the median (Omara et al., 2016). An aircraft mass balance study over northeastern
114 Pennsylvania calculated an emission rate between 0.18-0.41%, a number that accounted for emissions from the production,
115 processing, and transmission of the gas (Peischl et al., 2015). Both of these derived estimates fall below emission rates
116 calculated throughout other basins and are below the 3% threshold required for natural gas to be a smaller climate pollutant
117 in comparison to coal over a 20-year timescale. The low rates in the Marcellus compared to other regions could be the result
118 of a systematic difference within the Marcellus that leads to a more efficient extraction of natural gas. However, while useful
119 as a first-guess estimation, current studies performed in the region are based on relatively small sample sizes (1 aircraft mass
120 balance and 88 individual well measurements). A more thorough analysis of the emission rate in the Marcellus would
121 provide insight into regional differences in CH₄ emissions from different shale basins and help improve national estimates of
122 emissions from natural gas.

123 This study seeks to provide confidence in the emission rate for the northeastern Marcellus by performing the most
124 thorough top-down analysis of the northeastern Marcellus region to date. CH₄ measurements were taken from aircraft
125 observations across 10 flights in northeastern Pennsylvania. A new implementation of modelling CH₄ mole fractions is
126 developed to track complex plume structures associated with different emitters, and an optimal natural gas emission rate is
127 solved for each of the 10 flights. An aircraft mass balance technique is also conducted for 4 of the flights and natural gas
128 emission estimates from this method are compared to those calculated using the modelling technique. Using information on
129 the uncertainty with both methods, a regional emission rate is calculated for the natural gas industry in the northeastern
130 Marcellus region.

131 **2 Methods**

132 The objective of this study is to quantify CH₄ emissions coming from unconventional wells and compressor stations,
133 henceforth referred to as upstream natural gas emissions, in the northeastern Marcellus region (defined as the area contain

134 within 41.1-42.2°N 75.2-77.6°W, see Figure 1) through two different top-down methodologies. CH₄ observations from
135 aircraft data are collected for ten (10) individual flights over a three-week period in May 2015. These data are used to solve
136 for the upstream natural gas emission rate using an aircraft mass balance approach. Additionally, a CH₄ emissions inventory
137 for the region is compiled and input into an atmospheric transport model described below. CH₄ concentrations are modelled
138 for each flight, and the upstream natural gas emission rate within the model is optimized to create the best match between
139 aircraft observations and model projected enhancement, providing another estimate for the upstream natural gas emission
140 rate. The sections below detail the regional CH₄ inventory, the aircraft campaign, the transport model, the model
141 optimization technique, and the mass balance approach used in this study.

142

143 **2.1 Regional Methane Emission Inventory**

144 In this study we characterize emissions from the natural gas industry into five different sectors: emissions from wells,
145 emissions from compressor facilities, emissions from storage facilities, emissions from pipelines, and emissions in the
146 distribution sector.

147 To estimate CH₄ emissions from the production sector of the natural gas industry, data were first obtained on the
148 location and production rate of each unconventional well from the Pennsylvania Department of Environmental Protection
149 Oil and Gas Reporting website (PADEP, 2016) and the West Virginia Department of Environmental Protection (WVDEP,
150 2016). To convert the production rate into an emission rate, we need to assume a first-guess as to the expected leakage from
151 wells in the area. A first-guess natural gas emission rate of 0.13% was applied to the production value of each of the 7000+
152 producing unconventional wells based on the median rate from Omara et al., (2016). The natural gas emission rate was then
153 converted to a CH₄ emission rate by assuming a CH₄ composition in the natural gas of 95% (Peischl et al., 2015).

154 In addition to unconventional wells, the domain also contains more than 100,000 shallow conventional wells.
155 Annual conventional production rates for the year 2014 were obtained through the PADEP Oil and Gas Reporting website,
156 the WVDEP, and the New York Department of Environmental Conservation (NYDEC, 2016). Despite the large number of
157 wells, the average conventional well in PA produces 1% of the natural gas compared to its unconventional counterpart.
158 However, it is speculated that the older age of these wells and a lack of maintenance and care for them results in a higher
159 emission rate for these wells as a function of their production (Omara et al., 2016). A first-guess natural gas emission rate of
160 11% was applied to the production values of the conventional wells based on the median emission rate from the wells
161 sampled in Omara et al., (2016). Similar to the unconventional wells, the natural gas emission rate was then converted to a
162 CH₄ emission rate by assuming a CH₄ composition in the natural gas of 95%.

163 Compressor stations located within the basin are responsible for collecting natural gas from multiple well locations,
164 removing non-CH₄ hydrocarbons and other liquids from the flow, and regulating pressure to keep gas flowing along
165 gathering and transmission pipelines, and can be a potential source for methane emissions. Data for compressor station
166 locations and emissions comes from a dataset used in Marchese et al., (2015). A total of 489 compressor facilities are listed

167 for Pennsylvania, with 87% of the listed facilities also containing location data. Emissions for each compressor station are
168 calculated through two different methodologies. In the simplest case, a flat emission rate of 32.35 kg hr^{-1} is applied for each
169 station, the mean emission rate of a gathering facility in PA found in Marchese et al., (2015). In the more complex scenario,
170 the same emissions total is used as in the flat rate case, but is distributed among the compressor stations linearly as a function
171 of their energy usage. Wattage between compressors in our dataset can vary greatly, from 10 kW for small compressors to
172 7000 kW or more at large gathering facilities. Using the wattage as a proxy for emissions allows us to account for the size
173 and throughput of natural gas at each station and assumes larger stations will emit more natural gas compared to smaller
174 stations (Marchese et al., 2015).

175 Data on locations of underground storage facilities were obtained from the United States Energy Information
176 Administration (EIA, 2015). For each of these locations, a base emission rate of 96.7 kg hr^{-1} was applied according to the
177 average value emitted by a compressor station associated with an underground storage facility (Zimmerle et al., 2016).

178 To calculate pipeline emissions, data on pipeline locations needed to be collected. Information on transmission
179 pipelines, which connect gathering compressors to distribution networks, is provided by the Natural Gas Pipelines GIS
180 product purchased from Platts, a private organization which collects and creates various infrastructural layers for the natural
181 gas and oil industry (Platts, 2016). Gathering pipeline data, corresponding to the transfer of gas from wellheads to gathering
182 compressors, is nearly non-existent for PA with the exception of Bradford County, which maps out all gathering pipeline
183 infrastructure within the county border. In PA, information on the location of a gathering pipeline elsewhere is only available
184 where a gathering line crosses a stream or river. To account for gathering pipelines in the remainder of the state, a GIS model
185 was created using Bradford County pipelines map in addition to previously generated pipeline maps of Lycoming County
186 (Langlois et al., 2017) as a typical pattern to simulate connecting pipelines between unconventional wells throughout the
187 state (Figure 2). The resulting pattern follows the valley of the Appalachian Mountains, with larger pipelines crossing
188 through the state to connect the different branches of the network. These pipelines were then multiplied by an emission
189 factor of $0.043 \text{ kg per mile of pipe}$, the factor used for gathering pipeline leaks in the Inventory of U.S. Greenhouse Gas
190 Emissions and Sinks: 1990-2013 (EPA, 2015b).

191 CH_4 emissions from natural gas distribution sources, coal mines, and animal/animal waste were provided from
192 Maasackers et al., (2016), which takes national scale emissions from the EPA's greenhouse gas inventory for the year 2012
193 and transforms it into a $0.1^\circ \times 0.1^\circ$ emissions map for the continental U.S. For natural gas distribution emissions, various
194 pipeline data was collected at a state-level and emission factors were accounted for to calculate a total distribution emission
195 for the state. This emissions total was then distributed within the state proportional to the population density. Emission
196 estimates for coal are calculated using information from the Greenhouse Gas Reporting Program (GHGRP) for active mines
197 and the Abandoned Coal Mine Methane Opportunities Database for abandoned mines (EPA, 2008). State-level emissions
198 missions from enteric fermentation and manure management are provided in the EPA's inventory. These emissions were
199 segregated into higher resolutions using county-level data from the 2012 U.S. Census of Agriculture (USDA, 2012) and
200 land-type mapping.

201 Finally, the EPA's Greenhouse Gas Reporting Program dataset for the year 2014 was used to capture all other major
202 sources of CH₄ in the region otherwise unaccounted for, the majority of which are emissions from landfills and some
203 industrial sources (EPA, 2015a). Sources within the GHGRP that overlap with natural gas sources already accounted for
204 within our inventory were removed to prevent redundancy.

205 Although our emissions map used for the model runs did not account for potential CH₄ emissions from wetland
206 sources, a series of wetlands emission scenarios was obtained for the region using data from Bloom, et al., (2017). From this
207 dataset, wetland CH₄ emissions make up only 1% of all regional CH₄ emissions in the most extreme scenario, and thus we
208 assume their impact is negligible to this study.

209

210 **2.2 Aircraft Campaign**

211 Observations for this project were obtained from a 3-week aircraft campaign during the period of May 14th-June 3rd, 2015
212 and are available for public access (<https://doi.org/10.15138/G35K54>). The campaign was led by the Global Monitoring
213 Division (GMD) of the National Oceanic and Atmospheric Administration Earth Systems Research and Laboratory (NOAA
214 ESRL), in collaboration with the University of Michigan. During this period, the NOAA Twin Otter aircraft flew throughout
215 the northeast portion of Pennsylvania, providing a total of ten flights across nine days. The aircraft was equipped with a
216 Cavity Ring-Down Spectroscopic analyser (Picarro G2401-m) measuring CH₄, CO₂, CO, and water vapour mole fractions at
217 approximately 0.5Hz with a random error of 1 ppb, 0.1 ppm, 4 ppb, and 50 ppm respectively (Karion et al., 2013). GPS
218 location, horizontal winds, temperature, humidity, and pressure were also recorded at 1 Hz. The majority of observations for
219 each flight occurred during the afternoon hours at heights lower than 1500 m above ground level. Each flight contains at
220 least one vertical profile within and above the boundary layer, with temperature and water vapour observations from these
221 profiles used to estimate the atmospheric boundary layer height and ensure that the aircraft sampled air within the boundary
222 layer throughout the flight. Observations suspected of being located above the boundary layer top are flagged and removed
223 from all calculations.

224 Flight paths, wind speeds, and CH₄ observations for each of the 10 flights can be seen in Figure 3. For six of the ten
225 flights, a box pattern was flown around a large portion of unconventional natural gas wells in northeastern PA. These flights
226 were performed typically on days with a strong, steady wind, with a clearly defined upwind and downwind transect intended
227 for use in an aircraft mass balance calculation. Five of the six box-pattern flights were composed of two loops circling the
228 gas basin, allowing for two separate calculations of the upstream natural gas emission rate for the flight. On the remaining
229 four flights, raster patterns were performed to help identify spatial complexities of CH₄ emissions within the basin. All ten
230 flights were used in the model optimization calculation of the upstream natural gas emission rate.

231 2.3 Transport Model

232 The atmospheric transport model used in this study is the Advanced Weather Research and Forecasting (WRF) model
233 (WRF-ARW, Skamarock et al., 2008) version 3.6.1. The WRF configuration for the model physics used in this research
234 includes the use of: 1) the double-moment scheme (Thompson et al., 2004) for cloud microphysical processes, 2) the Kain-
235 Fritsch scheme (Kain and Fritsch 1990, Kain 2004) for cumulus parameterization on the 9-km grid, 3) the Rapid Radiative
236 Transfer Method for general circulation models (GCMs) (RRTMG, Mlawer et al., 1997, Iacono et al., 2008), 4) the level 2.5
237 TKE-predicting MYNN planetary boundary layer (PBL) scheme (Nakanishi and Niino 2006), and 5) the Noah 4-layer land-
238 surface model (LSM) that predicts soil temperature and moisture (Chen and Dudhia 2001, Tewari et al., 2004) in addition to
239 sensible and latent heat fluxes between the land surface and atmosphere.

240 The WRF model grid configuration used in this research contains two grids: 9- and 3-km (Figure 4), each with a
241 mesh of 202x202 grid points. The 9-km grid contains the mid-Atlantic region, the entire northeastern United States east of
242 Indiana, parts of Canada, and a large area of the northern Atlantic Ocean. The 3-km grid contains the entire state of
243 Pennsylvania and most of the state of New York. Fifty vertical terrain-following model layers are used, with the centre point
244 of the lowest model layer located at ~10 m above ground level. The thickness of the layers stays nearly constant with height
245 within the lowest 1 kilometre, with 26 model layers below 850 hPa (~1550 m AGL). One-way nesting is used so that
246 information from the coarse domain translates to the fine domain but no information from the fine domain translates to the
247 coarse domain.

248 The WRF modelling system used for this study also has four-dimensional data assimilation (FDDA) capabilities to
249 allow meteorological observations to be assimilated into the model (Deng et al., 2009). With WRF FDDA, observations are
250 assimilated through the entire simulation to ensure the optimal model solutions that combine both observation and the
251 dynamic solution, a technique referred to as dynamic analysis. Data assimilation can be accomplished by nudging the model
252 solutions toward gridded analyses based on observations (analysis nudging), or directly toward the individual observations
253 (observation nudging), with a multiscale grid-nesting assimilation framework typically using a combination of these two
254 approaches (Deng et al., 2009; Rogers et al., 2013).

255 FDDA (Deng et al., 2009) was used in this research, with the same strategy as used in Rogers et al., (2013). Both
256 analysis nudging and observation nudging were applied on the 9-km grid, and only observation nudging was applied on the
257 3-km grid. In addition to assimilating observations and using the North America Regional Reanalysis model as initial
258 conditions, we reinitialize the WRF model every five days, allowing 12 hours of overlapping period in consideration of
259 model spin-up period to prevent model errors from growing over long periods. The observation data types assimilated
260 include standard WMO surface and upper-air observations distributed by the National Weather Service (NWS), available
261 hourly for surface and 12-hourly for upper air, and the Aircraft Communications Addressing and Reporting System
262 (ACARS) commercial aircraft observations, available anywhere in space and time with low-level observations near the
263 major airports.

264 The WRF model used in this study enables the chemical transport option within the model allowing for the
265 projection of CH₄ concentrations throughout the domain. Surface CH₄ emissions used as input for the model come from our
266 CH₄ emissions inventory and are all contained within the 3-km nested grid. Each source of CH₄ within our inventory is
267 defined with its own tracer (Table 1), allowing for the tracking of each individual source's contribution to the overall
268 projected CH₄ enhancement within the model. For this study, CH₄ is treated as an inert gas. The potential for interaction with
269 the hydroxyl radical (OH), the main sink of CH₄, is neglected. A calculation assuming an above-average OH mole fraction
270 over a rural region of 0.5 pptv (Stone et al., 2012) and a reaction rate of 6.5×10^{-15} (Overend et al., 1975) produces a CH₄ sink
271 of 0.5ppb per hour. The duration of a flight can be up to 3 hours, leading to a potential loss of 1.5ppb over the course of a
272 flight. This loss is small but not insignificant. CH₄ plumes associated with natural gas during each flight ranged between 15-
273 70 ppb, and a change of 1.5ppb could theoretically impact observations by as much as 10% of the plume signal. However,
274 this decrease in the CH₄ mole fraction would likely have equal impacts on both the background CH₄ values as well as the
275 enhancement. Because emission calculations are based on the relative difference between the CH₄ background mole fraction
276 and the enhancement downwind, it would take a gradient in the oxidation of OH to impact the results. Considering this
277 relatively low destruction rate, the expected homogeneity of the sink across the region, and the difficulties associated with
278 the simulation of chemical loss processes, we assumed that the CH₄ mass is conserved throughout the afternoon and
279 therefore we ignored the impact of oxidation by OH.

280

281 **2.4 Model Optimization Technique**

282 **2.4.1 Model Optimization Methodology**

283 The objective of the model optimization technique is to solve for an emission rate as a percent of natural gas production that
284 creates the best match between modelled CH₄ concentration maps, provided by the transport model, with actual CH₄ mole
285 fraction observations provided by the aircraft data. The optimization process in this study was originally designed to solve
286 for natural gas emission from unconventional wells and emissions from compressor facilities separately. Because the flow
287 rate of natural gas being processed was not available for each compressor station, emissions at each facility were originally
288 scaled based on the size of the station. However, when running the transport model using this emissions map, enhancements
289 from the compressor stations produced plume structures nearly identical in shape to enhancements from the unconventional
290 wells due to the similar spatial distributions of these two tracers. Without distinct differences between the enhancement
291 patterns from each tracer, it becomes impossible to distinguish which emissions source must be adjusted to obtain the closest
292 match to the observations. For this reason, emissions from compressor facilities are merged with unconventional well
293 emissions in the optimized emission rate. Though the emission rate solved for in this experiment only uses the locations and
294 production for the unconventional wells, this optimized rate represents emissions from both the wells and compressor
295 facilities and are referred to as the modelled upstream natural gas emission rate. Midstream and downstream natural gas

296 processes (such as processing, transmission and distribution of the gas) and emissions from conventional wells are not solved
297 for in this study due to their minimal contribution (less than 5%) to CH₄ emissions in the region encompassed by the aircraft
298 campaign.

299 Using the transport model WRF-Chem, CH₄ atmospheric enhancements were generated for each flight using
300 different tracers to track different components to the overall CH₄ enhancement (e.g. animal/animal waste, distribution sector,
301 industries). From these concentration fields, the upstream natural gas emission rate was solved for each flight using a three-
302 step model optimization technique. First, a background concentration was determined for each flight and subtracted from the
303 observations to create a set of “observed CH₄ enhancements,” using

$$304 \quad X_{EnhO} = X_{Obs} - X_{bg} \quad , \quad (1)$$

305 where X_{Obs} is the CH₄ mole fraction observation from the aircraft, X_{bg} is a chosen background value for the flight, and
306 X_{EnhO} is the calculated CH₄ enhancement at each observation. In this study, the background value is defined as the ambient
307 CH₄ mole fraction over the region not accounted for by any of the sources within the model, with each flight having a unique
308 background value. Box-pattern flights containing 2 loops around the basin may have a different background value assigned
309 for each loop. To determine the background mole fraction, we start with the value of the observed mole fraction in the lowest
310 2nd percentile of all observations within the boundary layer for a given flight or loop. This chosen background value
311 represents the CH₄ mole fraction across the flight path from sources that are outside of our model domain. Because the
312 background value is meant to represent the CH₄ mole fraction outside the model domain that is otherwise unaccounted for in
313 our model, using the observations with the lowest CH₄ mole fraction is not always a sufficient definition for the background.
314 On certain days, CH₄ enhancements from sources within the model domain can form plumes with wide spatial coverage that
315 cover all observations during a flight. For example, during a flight the lowest CH₄ observations from the aircraft may be
316 1850 ppb, but the model simulation during that period indicates that all observations within the flight are being impacted by
317 at minimum a 20 ppb enhancement. In this case, we would set our background value for the flight at 1830 ppb, and say that
318 our 1850 ppb observations from the flight are a combination of an 1830 ppb background in addition to a 20 ppb
319 enhancement from sources within the model. By subtracting off this background value from our observations, we create a set
320 of “observed CH₄ enhancements” which can be directly compared to the model projected enhancements

321 The next step is to remove enhancements from this set that are not associated with emissions from upstream natural
322 gas using

$$323 \quad X_{GasO} = X_{EnhO} - X_{OtherM} \quad , \quad (2)$$

324 where X_{OtherM} is the modelled CH₄ enhancement at each observation from sources unrelated to upstream natural gas
325 processes, and X_{GasO} is the observation-derived CH₄ enhancement associated with upstream natural gas emissions for each
326 observation. In this step, each observed CH₄ enhancement has subtracted from it the projected non-natural gas enhancement
327 from the model (i.e. nearest grid point in space) using the corresponding model output time closest to the observation within

328 a 20-minute time interval. This creates a set of observed CH₄ enhancements related only to emissions from upstream gas
329 processes, filtering out potential signals from other CH₄ emitters and providing a set of observed enhancements that can be
330 directly compared to the projected upstream natural gas enhancement within the model. By subtracting these other sources
331 from the observations, we make the assumption that our emissions inventory is accurate for non-natural gas sources and that
332 the transport of these emissions is perfect, both of which are actually uncertain. Because errors exist in both the emissions
333 and transport, it is possible to create a negative observation-derived upstream gas enhancement if model-projected
334 enhancements from other sources are larger than the observation-derived enhancement. From the 10 flights, 16% of the
335 observation-derived enhancements are negative, but only 3% are negative by more than 5 ppb. To avoid solving for
336 unrealistic negative values, these negative observation-based upstream gas enhancements are set to 0. Errors associated with
337 this issue and other uncertainties with our inventory are examined further in the uncertainty analysis section of this paper.

338 In the final step, the upstream natural gas emission rate within the model is adjusted to create the best match
339 between the modelled upstream gas enhancement and observation-derived upstream gas enhancement using

$$340 \quad J = X_{GasO} - C * X_{GasM} \quad (3)$$

341 where X_{GasO} and X_{GasM} are the observed and modelled enhancement for each observation. In this equation, J is a cost
342 function we are trying to minimize by solving for a scalar multiplier C which, when applied to the modelled natural gas
343 enhancements, creates the smallest sum of the differences between the observation-derived upstream gas enhancement and
344 the modelled upstream enhancement. Because the emission rate within the model is linearly proportional to the model
345 enhancements, we can solve for the upstream natural gas emission rate that minimizes the cost function using

$$346 \quad E = 0.13 C \quad (4)$$

347 where 0.13 was the first guess upstream emission rate (in percent of production) used in the model, and E is the optimized
348 emission rate for the flight as a percentage of the natural gas production at each well. This final value represents an overall
349 emission rate associated with both unconventional wells and compressor stations across the region.

350 The decision to use a scalar cost function rather than the sum of squares is to account for possible misalignment
351 between any observed CH₄ plume and modelled plumes. There are two potential ways in which misalignment may occur.
352 One possibility is that the modelled wind direction differs from the true wind direction, leading to a plume in the model that
353 is off-centre in relation to the observed plume. The other possibility relates to how the model treats emissions from natural
354 gas as a uniform percent of production. In reality the emissions are more random in nature, and thus the plume may not
355 always develop over the wells with the largest production values. If a cost function is used that minimizes the sum of the
356 squares, any misalignment between the modelled and observed plume will result in the peak of the modelled plume aligning
357 with the height of the tail of the observed plume (Figure 5). Unless the observed plume aligns perfectly with the modelled
358 plume, the optimized emission rate using a sum of squares approach will always bias low. By using a scalar cost function,
359 we solve for an optimized emission rate that results in a plume with the same area under the curve compared to the observed

360 plume (Figure 5). This methodology is not impacted by any misalignment between the modelled vs. observed plumes,
361 preventing the low biases associated with a sum of squares minimization.

362

363 2.4.2 Model Optimization Uncertainty Assessment

364 For each of the ten flights, an uncertainty assessment was performed to obtain a range of likely upstream emission rates for
365 any individual flight. Five different sources of error were considered in this assessment: model wind speed error, model
366 boundary layer height error, CH₄ background error, CH₄ emission inventory error, and model/observation mismatch error.
367 These five sources of error vary substantially from flight to flight depending on conditions, and each can have significant
368 impacts on the total uncertainty (Table 4, 5).

369 Errors in the modelled wind speed and boundary layer height have impacts on our emission estimates that linearly
370 impact the results. If we assume a constant wind speed, a constant boundary layer height, and no entrainment of air from the
371 top of the boundary layer, we can use the following equation to understand their impacts.

$$372 \Delta C = \overline{F_0} \left(\frac{\Delta x}{U * D} \right) \quad (5)$$

373 where ΔC is the total CH₄ enhancement of the column of air contained within the boundary layer, $\overline{F_0}$ is the average emission
374 rate over the path the parcel travelled, Δx is the distance the column of air travelled, U is the wind speed and D is the
375 boundary layer height. Using this equation, we can see the linear relationship between the model wind speed, model
376 boundary layer height, and the calculated emission rate. As an example, if wind speeds in the model are biased low, natural
377 gas enhancements projected by the model would increase inversely. To compensate for this effect, the optimized emission
378 rate would decrease proportionally. A similar case can be made for bias in the boundary layer height. Both errors in the wind
379 speed and boundary layer height have known impacts on the optimized emission rate which can be corrected for, as long as
380 the errors of each are known.

381 To calculate the error in the model wind speed, we assume aircraft observations are truth and use

$$382 U_e = \frac{\overline{U}_m - \overline{U}_{obs}}{\overline{U}_{obs}} \quad (6)$$

383 where \overline{U}_{obs} is the mean observed wind speed by the aircraft across all points within the boundary layer, \overline{U}_m is the mean
384 modelled wind speed by the model across all points closest in time and space to each observation, and U_e is the wind speed
385 error percentage.

386 To compute the error in the modelled boundary layer height, the observed boundary layer height for each flight is
387 assumed to be the true boundary layer height and the boundary layer height percentage error, H_e , is estimated using:

$$388 H_e = \frac{\overline{H}_m - \overline{H}_{obs}}{\overline{H}_{obs}} \quad (7)$$

389 where \bar{H}_{obs} is the average observed boundary layer height across each of the aircraft profiles for a given flight, \bar{H}_m is the
390 model boundary layer height closest in time and space to the location of the observed profiles averaged over all profiles. For
391 both the observation and the model, boundary layer heights were determined by locating height of the potential temperature
392 inversion associated with the top of the boundary layer. On the May 22 flight where a potential temperature inversion could
393 not easily be identified in the observations, changes in water vapour, CO₂ and CH₄ mixing ratios were used to identify the
394 boundary layer top.

395 Errors in the model wind speed and boundary layer height are calculated for each of the ten flights. From these
396 errors, a corrected optimized emission rate is calculated for each flight using Eq. (8):

$$397 \quad E_{new} = \frac{E}{(1+U_e)(1+H_e)} \quad (8)$$

398 where E is the original emission rate and E_{new} is the corrected optimized upstream natural gas emission rate as a percent of
399 production.

400 In addition to errors related to wind speed and boundary layer height, we quantify three other sources of error in
401 each flight: errors in the selected CH₄ background value, errors in the CH₄ inventory, and errors associated with the overall
402 model performance (Table 5). Unlike the wind speed and boundary layer errors which have easily computable impacts on
403 the emission estimates, these other three sources of error and their impact on the optimized emission rate are more difficult
404 to quantify.

405 The background error relates to the value chosen for each flight which represents the ambient CH₄ concentration in
406 the boundary layer unrelated to emission sources within the model. In this study background values ranged from 1897-
407 1923ppb. Though background values should not have high variability during a 2-3 hour mid-afternoon flight, entrainment
408 from the boundary layer top can lead to the mixing in of tropospheric air that has different CH₄ mole fraction values from
409 those within the boundary layer, resulting in a change in the afternoon background value with time. Furthermore, for days on
410 which all aircraft observations (including those upwind of the unconventional wells) are impacted by various CH₄ plumes
411 predicted within the model, it is difficult to determine the background CH₄ concentration accurately. Additionally,
412 observations corresponding to locations with no modelled enhancement may in fact have been impacted by missing sources
413 in our inventory, highlighting the difficult nature of knowing with certainty where and what the background is for any given
414 flight. Understanding this uncertainty is crucial; any error in subtracting off the background value directly impacts each
415 observation's observed natural gas enhancement. For example, a background value of 1 ppb below the true background for a
416 given flight would add 1 ppb to each observed natural gas enhancement for all observations, creating a high bias with the
417 optimized upstream emission rate. To account for this error, each flight's optimization processes was rerun iterating the
418 background value by ± 5 ppb, and the ratio of the percent change in the emission rate compared to the original case was
419 defined as the resulting error in the emission rate due to background uncertainty. This ± 5 ppb background error range is an
420 estimate at the range of possible error in the background based on changes observed in the upwind measurements from each
421 of the flights and is meant to be a conservative estimate of the error. The impact this error can have in the emission rate

422 varies depending on the magnitude of the observed downwind enhancements during a flight. A plume containing a CH₄
423 enhancement of 50 ppb will have a smaller relative error from a 5 ppb change compared to one with an enhancement of only
424 10 ppb. Thus, days with high wind speeds and a high boundary layer height (and thus enhancements of a smaller magnitude)
425 tend to be affected the most by background errors.

426 Similar to background errors, errors from the CH₄ emissions inventory are difficult to quantify. In the model
427 optimization technique, we subtract out enhancements from sources unrelated to unconventional natural gas before solving
428 for the upstream gas emission rate. In doing so, we are making the assumption that our emissions inventory for sources
429 unrelated to upstream natural gas processes are accurate. In truth, each emission source in our inventory comes from a
430 different dataset and has its own unique error bounds, many of which are unknown. To simulate the potential errors
431 associated with unknowns in our inventory, we use a Monte Carlo approach and iterate the unconventional emissions
432 optimization approach for each flight 10,000 times, applying a random multiplier between 0-2 for each of the different
433 sources not associated with unconventional natural gas production. The resulting range of optimized natural gas emission
434 rates was fit to a Gaussian distribution and the 2σ emission range was calculated. Despite varying the emissions used in the
435 error analysis by 0 to 200% their original value, their impacts on the optimized natural gas emission rate are minimal on
436 most days due to the northeastern Marcellus region having very few emission sources not related to upstream natural gas
437 processes. Only for the flights on May 24th do we see errors from the inventory contribute significantly to the overall daily
438 error, when the coal plume in southwestern PA enters the centre of the study region and has a large role in the upstream
439 natural gas emission rate calculation for that day (Table 5).

440 The final source of error attempts to quantify the similarity of the pattern of modelled and observed natural gas
441 enhancements, referred to here as the model performance error. Figure 6 shows an example of two days, one of which the
442 model appears to recreate the observations, and the other of which the model poorly matches the shape of the observed
443 enhancements. Comparing these two simulations with no other information, we hypothesize that one should put more trust in
444 the upstream natural gas emission rate calculated for the flight whose modelled upstream enhancements match structurally
445 compared to the emission rate from the flight whose modelled enhancement bears little semblance to the observed
446 enhancement. The model performance error is designed to account for the trustworthiness of the optimized upstream
447 emission rate based on how well the model simulates a given day. The model performance error is calculated using a
448 modified normalized root mean squared error formula given in Eq. (9):

$$449 \quad e_{Perf} = \frac{\bar{\sigma}_{\Delta X}}{\Delta X_{gas}} \quad (9)$$

450 In this equation, $\bar{\sigma}_{\Delta X}$ is the standard deviation of the difference between the modelled and observation-derived upstream
451 natural gas CH₄ enhancement using the optimized emission rate, and ΔX_{gas} is the observed magnitude of enhancement from
452 the major natural gas plume observed in each flight. Here, ΔX_{gas} serves as a normalization factor to account for the varying
453 strength of the enhancement from flight to flight, and ensures that days with increased enhancements due to meteorological

454 conditions or true daily fluctuations in the upstream natural gas emissions do not proportionally impact the performance
455 error percentage. For example, a day with high winds and a deep boundary layer would produce smaller enhancements,
456 leading to a small $\bar{\sigma}_{\Delta X}$ regardless of model performance unless normalized by ΔX_{gas} .

457

458 2.5 Aircraft Mass Balance Method and Uncertainty Assessment

459 An aircraft mass balance calculation was performed for four applicable flights from the aircraft campaign as an alternative
460 method to calculate upstream natural gas emission rates independent of the transport model. The aircraft mass balance
461 approach uses the CH₄ enhancement between a downwind and upwind transect to calculate the total CH₄ flux of the area
462 contained between the two transects. We use the mass balance equation from Karion et al., (2013):

$$463 \quad E = \bar{U} \cos(\bar{\theta}) \int_{-b}^b \Delta X \int_{z=0}^{z_{top}} n_{air} dz dx \quad (10)$$

464 where E is the total flux (in mol s⁻¹) coming from the enclosed flight track, \bar{U} is the mean wind speed (in m s⁻¹), $\bar{\theta}$ is the mean
465 angle of the wind perpendicular to the flight track, ΔX is the CH₄ enhancement measured along the downwind flight track
466 from $-b$ to b (expressed as a mole fraction), n_{air} is the molar density of air within the boundary layer (in mol m⁻³), and each
467 of the integrals represents the summing over all air being measured within our transect in both the horizontal (x) and the
468 vertical (z). By simplifying further and using the mean enhancement along each downwind transect as the enhancement and
469 choosing z_{top} to be the top of the boundary layer, we can transform the previous equation into the following:

$$470 \quad E = 37.3LDU\Delta\bar{X}\cos(\bar{\theta}) \quad (11)$$

471 where L is the length of the transect (in meters), D is the depth of the boundary layer (in meters) found using observations
472 from vertical ascents during each flight, $\Delta\bar{X}$ is the mean enhancement across the transect (expressed as a mole fraction), \bar{U}
473 and $\bar{\theta}$ are the mean wind speed (in m s⁻¹) and wind direction relative to the angle of the transect, and 37.3 is the average
474 molar density of dry air within the boundary layer (in mol m⁻³) assuming an average temperature and pressure of 290K and
475 900hPa.

476 Of the 6 days from the aircraft campaign with a clearly defined upwind and downwind transect, one day (May 14th)
477 contained a surface high-pressure centre in the middle of the flight resulting in erratic wind patterns, and another day (May
478 25th) had CH₄ plumes from southwestern PA affecting portions the flight observations. These days were not used for a mass
479 balance, and calculations were performed for the remaining four box-pattern flights (May 22nd, May 23rd, May 28th, May
480 29th). From this list of remaining flights, three of them contained two loops around a portion of the Marcellus basin. A mass
481 balance was performed on each loop, resulting in a total of 7 mass balance calculations for the region across 4 days. Table 6
482 summarizes the results from the mass balance flights.

483 For each flight, a total flux within the box encompassed was calculated using Eq. (11). Using this flux, a natural gas
484 emission rate based on production from within the box was calculated using Eq. (12)

$$485 \quad E_{\%} = \frac{E - E_{other}}{P} \quad (12)$$

486 where E is the total flux from Eq. (11) (in kg hr^{-1}), E_{other} are the emissions enclosed in the box from sources not
487 related to upstream natural gas processes (in kg hr^{-1}), P is the total CH_4 from natural gas being produced within the box (in
488 kg hr^{-1}), and $E_{\%}$ is the resulting natural gas emission rate as a percent of total production within the box.

489 As an error analysis for the mass balance flight, we look at four potential sources of error (Table 7). One source of
490 uncertainty comes from the observed wind speed used in Eq. (11). For our experiment, we take the mean observed wind
491 speed from the aircraft and assume this value represents the mean wind speed within the entire box during the 2-4 hour
492 period it would take for air to travel from the upwind transect to the downwind transect. To understand the uncertainty and
493 biases associated with this assumption, we recreate wind observations along the flight path using values from WRF-Chem,
494 and compare the mean wind speed from the simulated observations to the mean model winds contained within the box
495 integrated throughout the boundary layer during the 3 hour period closest to the flight time. By making this comparison, we
496 are able to understand the representation error associated with treating the wind speed observations from the aircraft as the
497 wind speed within the entire box during the period it would take for air to cross from the upwind transect to the downwind
498 transect. On average, modelled wind speeds following the flight were 7% faster than integrated wind speeds within the box,
499 due to the inability for aircraft observations to account for slower wind speeds closer to the surface. This bias was removed
500 from each day's calculated wind speed. After accounting for the wind speed bias, the average error of the modelled wind
501 speed following the flight path compared to the modelled winds within the box was 3%. This 3% uncertainty was applied to
502 each flight and used as the potential uncertainty in the mean wind speed. Errors in the wind direction were neglected, as each
503 flight used in the mass balance completely surrounded the basin using downwind transects at multiple angles, and thus small
504 errors in the wind angle would result in a negligible net change on the total flux calculated.

505 Another source of uncertainty is error in the boundary layer height. For each flight, between 2-3 vertical profiles
506 were performed, and the mean height was used in Eq. (11). The standard deviation of different heights from each transect
507 was used as the uncertainty. On May 22nd, a boundary layer height could be interpreted from only one vertical transect. For
508 this day, we assume an uncertainty of ± 200 m ($\pm 9\%$).

509 Uncertainty in the CH_4 background mole fraction was estimated similar to the boundary layer height. On three of
510 the four flights, two upwind transects were performed. The mean observed CH_4 mole fraction between the two transects was
511 used as the background value for the entire flight, and the standard deviation between the loops was used as the uncertainty.
512 On both the May 23rd and May 28th flights, background differences between the two transects were less than the instrument
513 error of 1 ppb. On these days, we use the instrument error as the background error. On May 22nd, only one upwind transect
514 was usable for the calculation. For this day, we assume a conservative estimate in the uncertainty of the background of ± 5
515 ppb.

516 Finally, we assess uncertainty in the emissions inventory. After a CH_4 flux is calculated for each loop, emissions
517 from sources contained within the box that are not associated with upstream natural gas processes must be subtracted out to

518 solve for the upstream natural gas emission rate. Any errors associated with our inventory will result in a CH₄ source
519 attribution error. To account for the potentially large uncertainty with the emission sources in our inventory, we vary these
520 non-natural gas emissions by a factor of 2 to test the impact on the solved upstream natural gas emission rate. Because
521 northeastern Pennsylvania contains few sources of CH₄ emissions outside of natural gas production, the impact of this
522 uncertainty is typically less than 20% of the total emissions calculated within the box.

523 **3 Results**

524 **3.1 Methane Inventory**

525 From the first-guess CH₄ inventory created in this study, a total anthropogenic CH₄ emission rate of 2.76 Tg CH₄ year⁻¹ is
526 projected within our inner model domain (Figure 7) with values for individual source contributions shown in Table 2. This
527 total emissions estimate assumes a leak rate of 0.13% of gas production for unconventional wells, and does not account for
528 emissions from natural gas transmission and storage facilities outside of PA due to a lack of information available from other
529 states. Within the model domain, the area encompassing southwestern PA and northeastern WV stands out as the largest
530 contributor to CH₄ emissions, with emissions from conventional gas, unconventional gas, and coal mines all having
531 significant contributions to the total. In particular, the large emissions from coal make this region unique in comparison to
532 other shales. The EPA's Greenhouse Gas Reporting Program dataset for the year 2014 lists individual coal mines in the
533 southwestern portion of our domain as 8 of the top 10 CH₄ emitting facilities across the entire United States. This large area
534 source of CH₄ can have an impact on CH₄ concentrations hundreds of kilometres downwind and must be taken into account
535 when winds are from the southwest (Figure 8). Examples of this plume and its impacts on the aircraft campaign are
536 discussed in Section 3.2.1.

537

538 **3.2 Model Optimization Results**

539 **3.2.1 Case Studies**

540 From the aircraft campaign, a total of 10 flights across 9 days were used in the model optimization technique. For each one
541 of these flights, CH₄ concentration fields were produced using WRF-Chem, and the emission rate from upstream gas
542 processes was adjusted as outlined in the methods section to find the rate that best matches the total observed CH₄
543 enhancement. For box flights with two loops completed around the basin, emission rates were calculated for each loop
544 independent from one another and then averaged for the flight. Table 3 provides the general meteorology for the 10 flights.

545 During each of the observational periods, we use the transport model to project the mole fraction enhancement
546 across the region for each of the different CH₄ tracers (Figure 9). From these projections, we see three common sources of
547 CH₄ which can significantly influence the observed mole fractions in our study region of northeastern PA. The first is

548 emissions from unconventional gas in northeastern PA. Although the first-guess total emissions from upstream production in
549 the Marcellus are small compared to the overall contributions from other sources within the domain, their proximity to the
550 aircraft track results in unconventional gas having the largest contribution to observed enhancements throughout the domain
551 covered by most of the flights, often producing signals downwind of about 20-80 ppb above background levels. The second
552 most influential source of enhancements in our study region comes from various sources of CH₄ emissions located in
553 southwestern PA. Despite being more than 400 km away from our study region, large plumes from coal and other sources in
554 the southwestern corner of the state can contribute enhancements as high as 50 ppb across portions of the flight when winds
555 are from the southwest, affecting background measurements and masking signals from the unconventional gas. One final,
556 but less influential source of CH₄ enhancement is animal agriculture in southeastern PA. Lancaster County is home to
557 roughly 20% of all cattle in the state, with more than 200,000 cattle and calves as of 2012. A southerly wind can result in a
558 5-15 ppb enhancement across the flight path due to enteric fermentation and manure management from these cattle. Because
559 of coal, conventional gas, and cattle sources located south of the basin, signals from flights with a southerly component to
560 the wind can be difficult to interpret without modelling the projected plumes associated with these sources. Observations on
561 these days contrast to days with a northerly wind component, where a lack of CH₄ sources north of the study region results in
562 observations with a more clearly defined background and unconventional natural gas enhancement.

563 For each of the ten flights, variability in the model-observation offset was observed. The first loop of the May 29th
564 flight is the best example of a case where comparisons between the modelled and observed enhancements match closely after
565 optimization. For this flight, a box pattern was flown encompassing a majority of the unconventional wells in northeastern
566 PA, and enhancements were observed along the western and northern transects of the flight. Modelled enhancements from
567 sources unrelated to upstream gas emissions showed a broad CH₄ plume associated mostly with animal agriculture along the
568 western edge of the flight, and a smaller enhancement on the eastern edge associated with two landfills in the
569 Scranton/Wilkes-Barre urban corridor (Figure 10). Both of these enhancements are subtracted off from the observations to
570 produce a set of observation-derived enhancements due to upstream natural gas production and gathering facilities. Any
571 enhancements in this new observational dataset are located almost entirely along the northern transect of the flight, directly
572 downwind of the natural gas activity in the region. The observation-derived upstream gas enhancement is then directly
573 compared to the modelled upstream enhancement using its first guess emission rate, and an optimized upstream emission
574 rate of 0.26% of production (i.e. a doubling of the first guess) is calculated by minimizing the difference between the two
575 datasets (Figure 11).

576 The match between observed and modelled CH₄ enhancements on the first loop of the May 29th flight is closer than
577 any other flight in the campaign. The success of the model on this day is likely due to a number of ideal conditions. In
578 general, inconsistencies between the modelled and observed mean wind speeds and boundary layer heights can have a linear
579 bias on the projected enhancements, but for this flight differences between the observed and modelled wind speed and
580 boundary layer height were near 0 for both loops (Figure 12, 13). Observed wind directions throughout the course of the
581 flight had little directional spread and the averaged observed wind direction was only 9° different compared to modelled

582 values, resulting in a transport of the CH₄ plumes that the model was able to match well. Furthermore, the observed mean
583 wind speed was 4.6 m s⁻¹, a moderate wind which allows for a steady transport of any enhancements towards the downwind
584 transect, but not strong enough to dilute their magnitude, resulting in an easily observable enhancement downwind of the
585 basin. Finally, intrusions from sources unrelated to upstream gas were small on this day due to favourable wind conditions,
586 reducing the probability of incorrectly attributing the observed enhancements to the wrong source. Enhancements from
587 upstream natural gas processes were between 15-40 ppb along our downwind transect. By comparison, enhancements from
588 other sources were lower than 15 ppb along a majority of the flight, and most of these enhancements were located west of
589 the downwind transect, making them easier to identify and remove without unintentionally impacting enhancements from the
590 natural gas plume. All of these different factors likely contributed to producing a situation where the model was successfully
591 able to match CH₄ observations during the May 29th flight.

592 Flights that occurred on days with a southwest wind had a tendency to produce CH₄ observations that were
593 intuitively difficult to interpret due to convolved CH₄ sources in southwestern Pennsylvania. One of these complex
594 observation sets occurred during the late afternoon flight on May 24th, 2015 (Figure 14). Observations on this day show a
595 CH₄ enhancement that decreased with latitude, with higher CH₄ mole fractions observed farther south. Given the location of
596 the wells in the middle of the flight path and the WSW wind pattern in the region, this north/south CH₄ gradient is
597 unexpected and counterintuitive compared to where one would expect the enhancements to be based solely on the presence
598 of the gas industry in northeastern PA. However, through modelling each of the many contributors of CH₄ within our
599 inventory, we are able to recreate this latitudinal CH₄ gradient and better understand the observed patterns (Figure 14).
600 Throughout an 18-hour period leading up to the May 24th flight, winds from the SSW transport emissions from coal in
601 southwestern PA northeastward until they reach the centre of the state, where a westerly wind then shifts the plume across
602 the study region such that it only intersects the southern half of the flight path. Because of both the magnitude of the coal
603 emissions and an accumulation that occurred in the southwestern portion of the state during the previous night, the modelled
604 enhancement from the coal plume is substantial (>20 ppb) as it crosses over the flight path and covers up much of the signal
605 from upstream gas emissions. Nonetheless, the transport model is able to account for these far-reaching sources and attempt
606 to separate out their contribution to the observed enhancements. We are able to recreate the May 24th flight observations
607 more accurately than most other flights, with a correlation coefficient of 0.71 between the observations and model CH₄
608 values. Although the model successfully recreates the overall observed CH₄ pattern on this flight, attempting to match model
609 vs. observation-derived enhancements specifically from upstream natural gas contributions is much more difficult.
610 Contributions from non-natural natural gas sources are large such that they overwhelm much of the signal from local natural
611 gas sources. After subtracting out non-natural gas sources from the observations, the correlation specifically between
612 modelled and observation-derived upstream natural gas enhancements is only 0.11.

613 Despite the model's success at recreating observations from the May 24th late-afternoon flight, there is reason to be
614 careful when interpreting results on day with observations influenced by distant sources. In particular, some transport error is
615 unavoidable in atmospheric reanalyses, and the longer the time and distance a plume takes to reach the observations, the

616 more its position and magnitude will be susceptible to these errors. During the early May 24th flight, a small 50 km shift in
617 the location of the coal plume across the study region would change projected enhancements at some observations by as
618 much as 20 ppb. Furthermore, errors in the transport speed could create scenarios where the coal plume either arrives in the
619 study region too early or exits too late, creating a projected enhancement pattern that does not agree with the observations
620 (Figure 15). Additionally, inaccuracies with the emission estimates of non-unconventional gas sources in the inventory will
621 impact the magnitude of their CH₄ enhancements, creating additional errors in the optimization process when subtracting out
622 these enhancements from the observations. The early-afternoon May 24th flight and May 25th flight are both examples where
623 influences from CH₄ sources in southwest PA create complex structures in the enhancements, which the model is not able to
624 match as well as the late-afternoon flight on May 24th (Figure 16). And although observations and modelled enhancements
625 closely match throughout portions of these two flights, a slight shift in the modelled wind direction can lead to vastly
626 differing results due to the large offset small changes in the wind field can have on an emission source hundreds of
627 kilometres away. Thus, results from the flights on May 24th and May 25th should be taken with caution. A deeper analysis of
628 these errors can be found in Section 3.2.2.

629 3.2.2 Emission Rates and Uncertainty Assessment

630 Table 4 shows the wind speed and boundary layer height errors for each flight as well as the optimized and
631 corrected natural gas emission rates. On days where model performance was poor in regards to the wind speed and boundary
632 layer height, we can see changes in the corrected emission rate. For most days, this change is less than 20% different than the
633 original optimized emission rate. However, both May 14th and May 25th have corrected emission rates which are around a
634 factor of 2 different from their original value. Whether these corrected emission rates are more accurate than the original
635 optimized rates is debatable. To calculate these alternative emission rates, we must assume that the wind speeds and
636 boundary layer heights from our limited number of observations are the true values in the atmosphere, which may not be the
637 case. Regardless of which rate is more accurate for each flight, the overall 16% high bias in the model wind speed and the
638 -12% low bias in the model boundary layer result in compensating errors that cancel out, and the mean emission rates across
639 all flights end up similar. Thus, any errors associated with these two meteorological variables has a trivial impact on the
640 overall calculated emission rate for the region and the uncorrected emission rates are used for the final mean and uncertainty
641 calculations.

642 Table 5 summarizes the background error, inventory error, and model performance error, and assumes
643 independence between the three error sources to calculate the total uncertainty for each flight. The largest uncertainty exists
644 for the May 22nd flight, where an unexplained enhancement along the northern transect led to a poor match between the
645 modelled enhancements and the observed enhancements. This may explain the anomalously high optimized emission rate for
646 that day. Other flights with large uncertainty are those that occurred on May 24th, where enhancements from southwestern
647 PA are believed to be influencing large portions of the observations.

648 Based on the conservative methodology used to calculate these uncertainties, we assume the total uncertainty for
649 each flight represents a 2σ range of possible emission rates and calculate a weighted mean and a 2σ confidence interval for
650 the overall upstream emission rate across the ten flights. From this approach, we find a mean upstream emission rate of
651 0.36% of production and a 2σ confidence interval from 0.27-0.45% of production.

652 3.3 Aircraft Mass Balance Results

653 Calculated emission rates varied extensively between flights used for the mass balance analysis, ranging from 0.11% to
654 1.04% of natural gas production (Table 6). Comparing emission rates between loops on the same day, we see more
655 consistency in the values. This result is not surprising, as on each of the days with multiple loops, upwind and downwind
656 CH_4 concentrations patterns tended to be similar between loops. Thus, differences in the total emission rate are likely due to
657 either errors specific to each day (such as background variability, errors in meteorology) or real daily variability in the
658 upstream natural gas emission rate.

659 From Table 7, we can see the largest error with regards to the absolute uncertainty in the emission rate occurs on the
660 May 22nd flight. It is on this day where we have the largest uncertainty in the background value, with observations towards
661 the end of the flight becoming unusable due to a rapid and unexplained decrease in the CH_4 mole fraction of 8 ppb over a 30
662 minute period (Figure 17). This day also features the highest boundary layer height and fastest winds of all flights done in
663 this study, reducing the magnitude of the enhancement associated with the natural gas plume and thus amplifying the effects
664 an uncertain background has on the overall uncertainty of the calculated CH_4 flux. Uncertainty across the other three flights
665 is smaller, and results between individual loops on the May 23rd and May 28th flight provide more confidence in the
666 calculated flux for those days.

667 Using the mean estimated CH_4 emissions and uncertainty for each loop, we calculate a daily mean emission rate and
668 uncertainty for each of the four days. We then solve for an unweighted mean across the four flights to derive our overall
669 emissions estimate from the aircraft mass balance approach, and use the standard error of the flights to estimate the
670 uncertainty. In doing so, we derive a natural gas emission rate from upstream processes of 0.40% of production, with a 2σ
671 confidence interval from 0.08-0.72% of production. Here, we use the arithmetic mean rather than a weighted mean due to the
672 linear relationship between the size of the emission rate and the size of the errors. Because errors associated with ABL height
673 and wind speed have a proportional impact on the calculated emissions within the box, days with a high emissions estimate
674 produce large uncertainties relative to days with a small emission rate. Using a weighted mean approach assigns more weight
675 to the days with low estimated emissions, and produces an overall emission estimate too low and certain to have confidence
676 in (0.12 \pm 0.02 percent of gas production).

677

678 4 Discussion

679 4.1 Upstream Emission Rate

680 From this study, we estimate with a 2σ confidence interval an emission rate between 0.27-0.45% of gas production using the
681 model optimization method and 0.06-0.62% of gas production using the aircraft mass balance. Figure 18 provides the
682 emission range estimates from upstream natural gas processes using both the model optimization technique and mass balance
683 technique when applicable. Top-down studies of other basins in the U.S. have all found emission rates greater than 1% of
684 production, and thus the rates calculated for the northeastern Marcellus basin are the lowest observed yet, raising questions
685 as to why the values in this region appear to be low. One possibility may be related to the well efficiency of the northeastern
686 Marcellus region compared to other major shale plays (Table 8). In terms of gas production per unconventional well, the
687 Marcellus is the highest of all major basins in the U.S. Furthermore, the gas production per well increases by nearly a factor
688 of two when focusing specifically on Susquehanna and Bradford Counties in northeastern Pennsylvania where the majority
689 of the wells from this study are located (Figure 1). The large difference in production per well between the northeastern
690 Marcellus and other shales may partly explain the low emission rates as a percentage of production. Throughout this study,
691 we normalize natural gas emissions as a percentage of total production under the assumption that higher throughput of
692 natural gas in a system should lead to higher emissions in the system. However, if leaks are more influenced by the number
693 of components in operation rather than the throughput passing through the wells, a high production-per-well system such as
694 the unconventional wells in the northeastern Marcellus could end up having a very low emission rate as a percentage of
695 production, but a similar emission rate compared to other basins based on the number of wells, compressors, etc. A thorough
696 bottom-up study of the Marcellus region measuring emissions on a device level could provide an answer to this hypothesis.

697 Although we calculate a low emission rate for this region, rates calculated for May 22 and May 25 stand out as
698 outliers where emissions fall well-above our uncertainty bounds. It is possible that emissions from natural gas sources were
699 higher on these days compared to others. Releases of natural gas into the atmosphere from short timeframe events such as
700 liquids unloading and venting can add a temporal component to the emission rate. Such events occurring at an increased
701 frequency during the May 22 and May 25 flights could be responsible for the higher emission rates. However, these two days
702 both have issues that could have affected the optimized emission rate. On May 22, we observe a sudden drop in the observed
703 CH_4 values that is nearly as large as the main plume on that day, creating concerns about background concentrations. On
704 May 25, a southwesterly wind was present, and while the model showed the coal plume to be west of the flight path, a small
705 shift in the model wind direction would shift the coal plume over the region. For these reasons we are sceptical but not
706 dismissive of the high emission rates found during these two flights.

707

708

709 4.2 Advantages of Combining Observations with Model Output

710 One of the major advantages of using a chemical transport model to solve for natural gas emission rates compared to a
711 standard mass-balance approach is that the transport model is able to account for the complex and oftentimes non-uniform
712 plume structures originating from sources outside the flight path that can affect observations. When performing a mass
713 balance over a basin, it is assumed that the upwind transect is representative of the air exiting the downwind transect after
714 subtracting out all sources within the box. However, this assumption is only true if winds contained within the flight path are
715 in perfect steady state during the time it take for air to move from the upwind transect to the downwind transect, and that
716 measurements from the downwind transect occurred at a much later time so that the air being measured is the same air
717 measured from the upwind transect. These conditions are not easily achieved for regional scale mass balances due to the long
718 times needed for the air from the upwind transect to reach the downwind transect. As an example, from the four mass
719 balance flights performed for this study the average time for air to move from the upwind transect to the downwind transect
720 was 4 hours whereas the average time between the aircraft's upwind and downwind measurements was ~40 minutes. The
721 aircraft observations can be thought of as a snapshot in time, which can be problematic if large scale plumes from outside the
722 domain are moving through the region and impacting only certain portions of the observations during the flight's short
723 timeframe. By using a transport model for a domain much larger than that of the flight paths, we are able to track these far-
724 reaching plumes and identify situations where the background CH₄ concentrations may be spatially heterogeneous.

725 The potential usefulness of using a transport model alongside a mass balance calculation can best be demonstrated
726 from observations taken over the Marcellus during a 2013 aircraft campaign (Peischl et. al 2015). During this flight the
727 prevailing winds were from the WSW, and the largest CH₄ enhancements were observed along the western edge of the flight
728 path, upwind of the unconventional wells. Using our transport model, we are able to recreate the day of flight and attempt to
729 use our inventory and explain this feature (Figure 19). Comparisons between modelled output and observations show a 60
730 ppb CH₄ enhancement from coal and conventional wells in southwest PA stretching close to the western edge of the aircraft
731 observations, a plume structure similar to the one observed during the May 24th flight from our own study. Though this
732 plume does not initially align with the observed transect with the largest enhancements, we recognize that the coal and gas
733 plume travels for more than 20 hours (a distance of 400 km) from its source before reaching the flight path. If we allow for a
734 10% error in the transport speed and therefore advance the transport model by an additional two hours past the time in which
735 the aircraft observed these high values, we are able to line up the centre of the plume with the largest observed CH₄ mole
736 fractions along the western edge of the flight. In addition to the 60 ppb enhancement along the centre of the plume, the
737 model projects 20 ppb enhancements along the edges and in front of the plume centre. These smaller enhancements have an
738 influence along different portions of the flight which varies in magnitude, making it difficult to assess a proper background
739 CH₄ value upwind of the wells and potentially masking natural gas enhancements downwind of them. But by using a
740 transport model, we are able to see the potential impact of these far-reaching sources which would otherwise not be

741 considered in a regional mass balance and better understand the complex CH₄ plume structures which can occur in a given
742 region under specific wind conditions.

743 **5 Conclusion**

744 Using the model optimization technique presented in this study, we find a weighted mean natural gas emission rate from
745 unconventional production and gathering facilities of 0.36% of production with a 2 σ confidence interval from 0.27-0.45% of
746 production. This emission rate is supported by four mass balance calculations, which produce a mean of 0.40% and a 2 σ
747 confidence interval from of 0.08-0.72% of production. Applied to all the wells in our study region, this mean rate results in a
748 leakage rate of 20 Mg CH₄ hr⁻¹ for the year 2015. The emission rate found in this top-down study quantified as a percent of
749 production is significantly lower than rates found using top-down methodology at any other basin, and indicates the presence
750 of some fundamental difference in the northeastern Marcellus gas industry that is resulting in more efficient extraction and
751 processing of the natural gas.

752 The ten flights that took place in this study reveal large regional variations in the CH₄ enhancement patterns
753 depending on the prevailing wind direction. On days with a northwest wind, observed enhancements come primarily from
754 natural gas sources, and a small plume associated with it can be seen on the downwind leg of each flight with few
755 enhancements upwind of the wells. Flights that took place with winds conditions predominantly from the southwest were
756 more difficult to interpret. Plumes associated with coal and other potential sources of CH₄ in the southwestern Pennsylvania
757 create complex enhancement patterns affecting both the upwind and downwind portions of the flight, making both the
758 background CH₄ mole fraction and enhancements from the gas industry difficult to interpret. The stark difference between
759 observations that occurred with a northwest wind compared to a southwest wind illustrates the importance of having multiple
760 flights across days with various wind conditions to better understand the major influences on CH₄ concentrations throughout
761 a region. The regional influences in Pennsylvania also demonstrate the utility of deriving an emissions inventory that
762 provides input data to drive a transport model, allowing one to forecast CH₄ mole fractions on difficult days and better
763 understand the daily uncertainties associated with heterogeneous background conditions.

764 Though this study presented observations from ten flights over a three-week period, it is not able to account for the
765 potential of long term temporal variability in the emission rates. In May 2015 when the flights took place, the entire
766 Marcellus basin was nearing peak production and active drilling and hydraulic fracturing was still ongoing in the region. By
767 mid-2016, the rate of drilling of new wells in the northeast Marcellus had decreased and natural gas production had begun to
768 decline in the area. A snapshot of the emission rate during one month of a basin in its peak production is insufficient to
769 characterize emissions from an area that is likely to be producing and transporting gas at various intensities for decades. We
770 need to quantify the long-term climatological impacts of gas production. Future work examining the temporal variability of
771 CH₄ emissions within natural gas basins would complement short-term, high-intensity studies such as this one, and aid with
772 understanding how well the calculated emission rates represent the gas basin over the course of time.

773 **Acknowledgements**

774 This work has been funded by the U.S. Department of Energy National Energy Technology Laboratory (project DE-
775 FE0013590). We thank in-kind contributions from the Global Monitoring Division of the National Oceanic and Atmospheric
776 Administration, and from the Earth and Environmental Systems Institute, the Department of Meteorology and Atmospheric
777 Science, and the College of Earth and Mineral Science of The Pennsylvania State University. We also want to thank the
778 Pennsylvania College of Technology in Williamsport, PA for access to their Technology Aviation Center facilities during
779 the aircraft campaign. We also want to thank Lillie Langlois from the Department of Ecosystem Science and
780 Management for sharing pipeline information, Anthony J. Marchese and Dan Zimmerle (Colorado State University) for
781 information on compressor stations, Jeff Peischl for sharing data from his 2013 flight campaign, and Bernd Haupt (Penn
782 State University) for data processing and management during the project. Finally, we would like to thank Dennis and Joan
783 Thomson for their creation and continued support of the Thomson Distinguished Graduate Fellowship.

784 **References**

- 785 Alvarez, R. A., Pacala, S. W., Winebrake, J. J., Chameides, W. L., and Hamburg, S. P.: Greater focus needed on methane
786 leakage from natural gas infrastructure, *Proceedings of the National Academy of Sciences*, 109, 6435-6440,
787 10.1073/pnas.1202407109, 2012.
- 788
- 789 Bloom, A. A., Bowman, K., Lee, M., Turner, A. J., Schroeder, R., Worden, J. R., Weidner, R., McDonald, K. C., and Jacob,
790 D. J.: A global wetland methane emissions and uncertainty dataset for atmospheric chemical transport models,
791 *Geosci. Model Dev.*, 10.5194/gmd-10-2141-2017, 2017.
- 792
- 793 Bradford County: Maps of Natural Gas Development in Bradford County, available at:
794 <http://www.bradfordcountypa.org/index.php/natural-gas-information>.
- 795
- 796 Bousquet, P., Ciais, P., Miller, J. B., Dlugokencky, E. J., Hauglustaine, D. A., Prigent, C., Van der Werf, G. R., Peylin, P.,
797 Brunke, E. G., Carouge, C., Langenfelds, R. L., Lathiere, J., Papa, F., Ramonet, M., Schmidt, M., Steele, L. P.,
798 Tyler, S. C., and White, J.: Contribution of anthropogenic and natural sources to atmospheric methane variability,
799 *Nature*, 443, 439-443, http://www.nature.com/nature/journal/v443/n7110/supinfo/nature05132_S1.html, 2006.
- 800
- 801 Brandt, A. R., Heath, G. A., Kort, E. A., O'Sullivan, F., Pétron, G., Jordaan, S. M., Tans, P., Wilcox, J., Gopstein, A. M.,
802 Arent, D., Wofsy, S., Brown, N. J., Bradley, R., Stucky, G. D., Eardley, D., and Harriss, R.: Methane Leaks from
803 North American Natural Gas Systems, *Science*, 343, 733-735, 10.1126/science.1247045, 2014.
- 804
- 805 Cambaliza, M. O. L., Shepson, P. B., Caulton, D. R., Stirm, B., Samarov, D., Gurney, K. R., Turnbull, J., Davis, K. J.,
806 Possolo, A., Karion, A., Sweeney, C., Moser, B., Hendricks, A., Lauvaux, T., Mays, K., Whetstone, J., Huang, J.,
807 Razlivanov, I., Miles, N. L., and Richardson, S. J.: Assessment of uncertainties of an aircraft-based mass balance
808 approach for quantifying urban greenhouse gas emissions, *Atmos. Chem. Phys.*, 14, 9029-9050, 10.5194/acp-14-
809 9029-2014, 2014.
- 810
- 811 Chen, F., and Dudhia, J.: Coupling an Advanced Land Surface–Hydrology Model with the Penn State–NCAR MM5
812 Modeling System. Part I: Model Implementation and Sensitivity, *Monthly Weather Review*, 129, 569-585,
813 10.1175/1520-0493(2001)129<0569:caalsh>2.0.co;2, 2001.
- 814
- 815 Conley, S., Franco, G., Faloona, I., Blake, D. R., Peischl, J., and Ryerson, T. B.: Methane emissions from the 2015 Aliso
816 Canyon blowout in Los Angeles, CA, *Science*, 10.1126/science.aaf2348, 2016.
- 817
- 818 Deng, A., Stauffer, D., Gaudet, B., Dudhia, J., Hacker, J., Bruyere, C., Wu, W., Vandenberghe, F., Liu, Y., and Bourgeois,
819 A.: Update on WRF-ARW end-to-end multi-scale FDDA system, 10th Annual WRF Users' Workshop, Boulder,
820 CO, June 23, 2009.
- 821
- 822 Deng, A., Gaudet, B., Dudhia, J., and Alapaty, K.: Implementation and Evaluation of a New Shallow Convection Scheme in
823 WRF, 94th American Meteorological Society Annual Meeting, Atlanta, GA, February 2-6, 2014.
- 824
- 825 EIA: Annual Energy Outlook 2012 with Projections to 2035, available at:
826 [http://www.eia.gov/forecasts/aeo/pdf/0383\(2012\).pdf](http://www.eia.gov/forecasts/aeo/pdf/0383(2012).pdf), 2012.
- 827
- 828 EIA: Layer Information for Interactive State Maps, available at: https://www.eia.gov/maps/layer_info-m.cfm, 2015
- 829
- 830 EIA: Shale in the United States, available at: https://www.eia.gov/energyexplained/index.cfm?page=natural_gas_where,
831 2016a
- 832

833 EIA: Monthly Energy Review: June 2016. [Available online at
834 <http://www.eia.gov/totalenergy/data/monthly/archive/00351607.pdf> , 2016b.
835

836 EPA: Abandoned Coal Mine Methane Opportunities Database, available at: [https://www.epa.gov/cmop/abandoned-](https://www.epa.gov/cmop/abandoned-underground-mines)
837 [underground-mines](https://www.epa.gov/cmop/abandoned-underground-mines), 2008.
838

839 EPA: Greenhouse Gas Reporting Program 2014, available at: [https://www.epa.gov/ghgreporting/ghg-reporting-program-](https://www.epa.gov/ghgreporting/ghg-reporting-program-data-sets)
840 [data-sets](https://www.epa.gov/ghgreporting/ghg-reporting-program-data-sets), 2015a.
841

842 EPA: Inventory of US Greenhouse Gas Emissions and Sinks: 1990-2013 Annex 3.6, available at:
843 <https://www.epa.gov/ghgemissions/inventory-us-greenhouse-gas-emissions-and-sinks-1990-2013>, 2015b.
844

845 EPA: Inventory of US Greenhouse Gas Emissions and Sinks: 1990-2014 Annex 2.2, available at:
846 <https://www.epa.gov/ghgemissions/inventory-us-greenhouse-gas-emissions-and-sinks-1990-2014>, 2016.
847

848 Frankenberg C., Thorpe, A. K., Thompson, D. R., Hulley, G., Kort, E. A., Vance, N., Borchardt, J., Krings, T., Gerilowski,
849 K., Sweeney, C., Conley, S., Bue, B. D., Aubrey, A. D., Hook, S., and Green, R. O.: Airborne methane remote
850 measurements reveal heavy-tail flux distribution in Four Corners region, *Proceedings of the National Academy of*
851 *Sciences*, 113, 9734-9739, 2016.
852

853 Hughes, J. D.: *Drilling Deeper: A Reality Check on US Government Forecasts for a Lasting Tight Oil & Shale Gas Boom*,
854 Post Carbon Institute, Santa Rosa, California, 2014.
855

856 Iacono, M. J., Delamere, J. S., Mlawer, E. J., Shephard, M. W., Clough, S. A., and Collins, W. D.: Radiative forcing by long-
857 lived greenhouse gases: Calculations with the AER radiative transfer models, *Journal of Geophysical Research:*
858 *Atmospheres*, 113, 10.1029/2008jd009944, 2008.
859

860 Jimenez, P. A., Hacker, J. P., Dudhia, J., Haupt, S. E., Ruiz-Arias, J. A., Gueymard, C. A., Thompson, G., Eidhammer, T.,
861 and Deng, A.: WRF-Solar: Description and Clear-Sky Assessment of an Augmented NWP Model for Solar Power
862 Prediction, *Bulletin of the American Meteorological Society*, 97, 1249-1264, 10.1175/bams-d-14-00279.1, 2016.
863

864 Jiménez, P. A., Alessandrini, S., Haupt, S. E., Deng, A., Kosovic, B., Lee, J. A., and Monache, L. D.: The Role of
865 Unresolved Clouds on Short-Range Global Horizontal Irradiance Predictability, *Monthly Weather Review*, 144,
866 3099-3107, 10.1175/mwr-d-16-0104.1, 2016.
867

868 Kain, J. S., and Fritsch, J. M.: A One-Dimensional Entraining/Detraining Plume Model and Its Application in Convective
869 Parameterization, *Journal of the Atmospheric Sciences*, 47, 2784-2802, 10.1175/1520-
870 0469(1990)047<2784:aodepm>2.0.co;2, 1990.
871

872 Kain, J. S.: The Kain–Fritsch Convective Parameterization: An Update, *Journal of Applied Meteorology*, 43, 170-181,
873 10.1175/1520-0450(2004)043<0170:tkcpau>2.0.co;2, 2004.
874

875 Karion, A., Sweeney, C., Pétron, G., Frost, G., Michael Hardesty, R., Kofler, J., Miller, B. R., Newberger, T., Wolter, S.,
876 Banta, R., Brewer, A., Dlugokencky, E., Lang, P., Montzka, S. A., Schnell, R., Tans, P., Trainer, M., Zamora, R.,
877 and Conley, S.: Methane emissions estimate from airborne measurements over a western United States natural gas
878 field, *Geophysical Research Letters*, 40, 4393-4397, 10.1002/grl.50811, 2013.
879

880 Karion, A., Sweeney, C., Kort, E. A., Shepson, P. B., Brewer, A., Cambaliza, M., Conley, S. A., Davis, K., Deng, A.,
881 Hardesty, M., Herndon, S. C., Lauvaux, T., Lavoie, T., Lyon, D., Newberger, T., Pétron, G., Rella, C., Smith, M.,

882 Wolter, S., Yacovitch, T. I., and Tans, P.: Aircraft-Based Estimate of Total Methane Emissions from the Barnett
883 Shale Region, *Environmental Science & Technology*, 49, 8124-8131, 10.1021/acs.est.5b00217, 2015.
884

885 Lamb, B. K., Cambaliza, M. O. L., Davis, K. J., Edburg, S. L., Ferrara, T. W., Floerchinger, C., Heimburger, A. M. F.,
886 Herndon, S., Lauvaux, T., Lavoie, T., Lyon, D. R., Miles, N., Prasad, K. R., Richardson, S., Roscioli, J. R., Salmon,
887 O. E., Shepson, P. B., Stirm, B. H., and Whetstone, J.: Direct and Indirect Measurements and Modeling of Methane
888 Emissions in Indianapolis, Indiana, *Environmental Science & Technology*, 50, 8910-8917,
889 10.1021/acs.est.6b01198, 2016.
890

891 Langlois, L. A., Drohan, P. J., and Brittingham, M. C.: Linear infrastructure drives habitat conversion and forest
892 fragmentation associated with Marcellus shale gas development in a forested landscape. *Journal of Environmental*
893 *Management*. 197, 167-176, 10.1016/j.jenvman.2017.03.045. 2017.
894

895 Lauvaux, T., Uliasz, M., Sarrat, C., Chevallier, F., Bousquet, P., Lac, C., Davis, K. J., Ciais, P., Denning, A. S., and Rayner,
896 P. J.: Mesoscale inversion: first results from the CERES campaign with synthetic data, *Atmos. Chem. Phys.*, 8,
897 3459-3471, 10.5194/acp-8-3459-2008, 2008.
898

899 Maasackers, J. D., Jacob, D. J., Sulprizio, M. P., Turner, A. J., Weitz, M., Wirth, T., Hight, C., DeFigueiredo, M., Desai, M.,
900 Schmeltz, R., Hockstad, L., Bloom, A. A., Bowman, K. W., Jeong, S., and Fischer, M. L.: Gridded National
901 Inventory of U.S. Methane Emissions, *Environmental Science & Technology*, 50, 13123-13133,
902 10.1021/acs.est.6b02878, 2016.
903

904 Marchese, A. J., Vaughn, T. L., Zimmerle, D. J., Martinez, D. M., Williams, L. L., Robinson, A. L., Mitchell, A. L.,
905 Subramanian, R., Tkacik, D. S., Roscioli, J. R., and Herndon, S. C.: Methane Emissions from United States Natural
906 Gas Gathering and Processing, *Environmental Science & Technology*, 49, 10718-10727, 10.1021/acs.est.5b02275,
907 2015.
908

909 Mays, K. L., Shepson, P. B., Stirm, B. H., Karion, A., Sweeney, C., and Gurney, K. R.: Aircraft-Based Measurements of the
910 Carbon Footprint of Indianapolis, *Environmental Science & Technology*, 43, 7816-7823, 10.1021/es901326b, 2009.
911

912 Mlawer, E. J., Taubman, S. J., Brown, P. D., Iacono, M. J., and Clough, S. A.: Radiative transfer for inhomogeneous
913 atmospheres: RRTM, a validated correlated-k model for the longwave, *Journal of Geophysical Research:*
914 *Atmospheres*, 102, 16663-16682, 10.1029/97jd00237, 1997.
915

916 Myhre, G., Shindell, D., Bréon, F.-M., Collins, W., Fuglestedt, J., Huang, J., Koch, D., Lamarque, J.-F., Lee, D., and
917 Mendoza, B.: Anthropogenic and natural radiative forcing, *Climate change*, 423, 2013.
918

919 Nakanishi, M., and Niino, H.: An improved Mellor–Yamada level-3 model: Its numerical stability and application to a
920 regional prediction of advection fog, *Boundary-Layer Meteorology*, 119, 397-407, 2006.
921

922 NYDEC: NY 2014 Oil & Gas Production Data: available at: <http://www.dec.ny.gov/energy/36159.html>, 2016.
923

924 Omara, M., Sullivan, M. R., Li, X., Subramanian, R., Robinson, A. L., and Presto, A. A.: Methane Emissions from
925 Conventional and Unconventional Natural Gas Production Sites in the Marcellus Shale Basin, *Environmental*
926 *Science & Technology*, 50, 2099-2107, 10.1021/acs.est.5b05503, 2016.
927

928 Overend, R. P., Paraskevopoulos, G., and Cvetanović, R. J.: Rates of OH Radical Reactions. I. Reactions with H₂, CH₄,
929 C₂H₆, and C₃H₈ at 295 K, *Canadian Journal of Chemistry*, 53, 3374-3382, 10.1139/v75-482, 1975.
930

931 PADEP: PA Oil and Gas Well Historical Production Report, available at:
932 http://www.depreportingservices.state.pa.us/ReportServer/Pages/ReportViewer.aspx?%2fOil_Gas%2fOil_Gas_Wel
933 [l_Historical_Production_Report](http://www.depreportingservices.state.pa.us/ReportServer/Pages/ReportViewer.aspx?%2fOil_Gas%2fOil_Gas_Wel), 2016.
934

935 Peischl, J., Ryerson, T. B., Aikin, K. C., de Gouw, J. A., Gilman, J. B., Holloway, J. S., Lerner, B. M., Nadkarni, R.,
936 Neuman, J. A., Nowak, J. B., Trainer, M., Warneke, C., and Parrish, D. D.: Quantifying atmospheric methane
937 emissions from the Haynesville, Fayetteville, and northeastern Marcellus shale gas production regions, *Journal of*
938 *Geophysical Research: Atmospheres*, 120, 2119-2139, 10.1002/2014jd022697, 2015.
939

940 Pétron, G., Frost, G., Miller, B. R., Hirsch, A. I., Montzka, S. A., Karion, A., Trainer, M., Sweeney, C., Andrews, A. E.,
941 Miller, L., Kofler, J., Bar-Ilan, A., Dlugokencky, E. J., Patrick, L., Moore, C. T., Ryerson, T. B., Siso, C.,
942 Kolodzey, W., Lang, P. M., Conway, T., Novelli, P., Masarie, K., Hall, B., Guenther, D., Kitzis, D., Miller, J.,
943 Welsh, D., Wolfe, D., Neff, W., and Tans, P.: Hydrocarbon emissions characterization in the Colorado Front Range:
944 A pilot study, *Journal of Geophysical Research: Atmospheres*, 117, 10.1029/2011jd016360, 2012.
945

946 Platts: Maps and Geospatial Data: available at: <http://www.platts.com/maps-geospatial>, 2016.
947

948 Rogers, R., Deng, A., Stauffer, D., Jia, Y., Soong, S., Tanrikulu, S., Beaver, S., and Tran, C.: Fine particulate matter
949 modeling in Central California. Part I: Application of the Weather Research and Forecasting model, 91th Annual
950 Meeting, 2011.
951

952 Ryerson, T. B., Trainer, M., Holloway, J. S., Parrish, D. D., Huey, L. G., Sueper, D. T., Frost, G. J., Donnelly, S. G.,
953 Schauffler, S., Atlas, E. L., Kuster, W. C., Goldan, P. D., Hübler, G., Meagher, J. F., and Fehsenfeld, F. C.:
954 Observations of Ozone Formation in Power Plant Plumes and Implications for Ozone Control Strategies, *Science*,
955 292, 719-723, 10.1126/science.1058113, 2001.
956

957 Schwietzke, S., Griffin, W. M., Matthews, H. S., and Bruhwiler, L. M. P.: Natural Gas Fugitive Emissions Rates Constrained
958 by Global Atmospheric Methane and Ethane, *Environmental Science & Technology*, 48, 7714-7722,
959 10.1021/es501204c, 2014.
960

961 Smith, M. L., Kort, E. A., Karion, A., Sweeney, C., Herndon, S. C., and Yacovitch, T. I.: Airborne Ethane Observations in
962 the Barnett Shale: Quantification of Ethane Flux and Attribution of Methane Emissions, *Environmental Science &*
963 *Technology*, 49, 8158-8166, 10.1021/acs.est.5b00219, 2015.
964

965 Skamarock, W. C., Klemp, J. B., Dudhia, J., Gill, D. O., Barker, D. M., Wang, W., and Powers, J. G.: A description of the
966 advanced research WRF version 2, DTIC Document, 2005.
967

968 Stone, D., Whalley, L. K., and Heard, D. E.: Tropospheric OH and HO₂ radicals: field measurements and model
969 comparisons, *Chemical Society Reviews*, 41, 6348-6404, 10.1039/c2cs35140d, 2012.
970

971 Sweeney, C., Karion, A., Kort, E. A., Smith, M. L., Newberger T., Schwietzke, S., Wolter, S., and Lauvaux, T.: Aircraft
972 Campaign Data over the Northeastern Marcellus Shale, May-June 2015, Version: 2017-03-29, Path:
973 <https://doi.org/10.15138/G35K54>, 2015
974

975 Tewari, M., Chen, F., Wang, W., Dudhia, J., LeMone, M., Mitchell, K., Ek, M., Gayno, G., Wegiel, J., and Cuenca, R.:
976 Implementation and verification of the unified NOAA land surface model in the WRF model, 20th conference on
977 weather analysis and forecasting/16th conference on numerical weather prediction, 2004.
978

979 Thompson, G., Field, P. R., Rasmussen, R. M., and Hall, W. D.: Explicit Forecasts of Winter Precipitation Using an
980 Improved Bulk Microphysics Scheme. Part II: Implementation of a New Snow Parameterization, Monthly Weather
981 Review, 136, 5095-5115, 10.1175/2008mwr2387.1, 2008.
982
983 USDA: Census Ag Atlas Maps, available at:
984 https://www.agcensus.usda.gov/Publications/2012/Online_Resources/Ag_Atlas_Maps/Livestock_and_Animals/,
985 2012.
986
987 White, W. H., Anderson, J. A., Blumenthal, D. L., and Wilson, W. E., Formation and transport of secondary air-pollutants:
988 Ozone and aerosols in St. Louis urban plume: Science 194, 187-189, 10.1126/science.959846, 1976.
989
990 WVDEP: WV Oil and Gas Database and Map Information, available at: [http://www.dep.wv.gov/oil-and-](http://www.dep.wv.gov/oil-and-gas/databaseinfo/Pages/default.aspx)
991 [gas/databaseinfo/Pages/default.aspx](http://www.dep.wv.gov/oil-and-gas/databaseinfo/Pages/default.aspx), 2016.
992
993 Zavala-Araiza, D., Lyon, D., Alvarez, R. A., Palacios, V., Harriss, R., Lan, X., Talbot, R., and Hamburg, S. P.: Toward a
994 Functional Definition of Methane Super-Emitters: Application to Natural Gas Production Sites, Environmental
995 Science & Technology, 49, 8167-8174, 10.1021/acs.est.5b00133, 2015
996
997 Zavala-Araiza, D., Alvarez, R. A., Lyon, D. R., Allen, D. T., Marchese, A. J., Zimmerle, D. J., and Hamburg, S. P.: Super-
998 emitters in natural gas infrastructure are caused by abnormal process conditions, Nature Communications, 8, 14012,
999 10.1038/ncomms14012, 2017.
1000
1001 Zimmerle, D. J., Williams, L. L., Vaughn, T. L., Quinn, C., Subramanian, R., Duggan, G. P., Willson, B., Opsomer, J. D.,
1002 Marchese, A. J., Martinez, D. M., and Robinson, A. L.: Methane Emissions from the Natural Gas Transmission and
1003 Storage System in the United States, Environmental Science & Technology, 49, 9374-9383,
1004 10.1021/acs.est.5b01669, 2015.

Table 1: List of tracers used in the transport model.

Tracer #	Name	Description of source
1	Unconventional Wells	Emissions from unconventional wells.
2	Storage Facilities	Emissions from compressors associated with natural gas storage.
3	Pipelines	Emissions from gathering and transmission pipelines
4	Distribution	Emissions from the distribution sector of the natural gas industry.
5	Conventional Wells	Emissions from conventional wells.
6	Landfills/Other	Emissions from landfills and uncharacterized industrial sources.
7	Coal	Emissions from active and abandoned coal mining.
8	Animals/Waste	Emissions from enteric fermentation and manure management
9	Production Compressors (HP)	Emissions from compressor stations characterized as “production”. Emissions scaled linearly with wattage.
10	Gathering Compressors (HP)	Emissions from compressor stations characterized as “gathering”. Emissions scaled linearly with wattage.
11	Other Compressors (HP)	Emissions from all other compressor stations. Emissions scaled linearly with wattage.
12	Production Compressors (C)	Emissions from compressor stations characterized as “production”. Emissions constant among compressors.
13	Gathering Compressors (C)	Emissions from compressor stations characterized as “gathering”. Emissions constant among compressors.
14	Other Compressors (C)	Emissions from all other compressor stations. Emissions constant among compressors.

Table 2: Annual emission rate totals from anthropogenic sources within the innermost model domain based on values from the inventory within this study

Source	Total Emission Rate (Gg CH ₄ year ⁻¹)
Unconventional Wells	125
Conventional Wells	607
Gathering Compressor Facilities	118
Storage Facilities	69
Gathering/Transmission Pipelines	8
Natural Gas Distribution	213
Underground, Surface, and Abandoned Coal Mines	831
Enteric Fermentation/Manure Management	371
Landfills	420
Total	2762

Table 3: Meteorological statistics from the May 2015 flight campaign.

Day	Flight Pattern	# of Loops	# of Vertical Profiles	ABL Depth (m)	Mean Observed Wind Speed (m/s)	Mean Observed Wind Direction	Model Background Value (ppm)
May 14	Box	1	2	1300	2.9	30°	1.908
May 21	Raster	N/A	2	1300	3.9	231°	1.905
May 22	Box	2	2	2300	10.1	300°	1.910
May 23	Box	2	2	1400	4.4	276°	1.906
May 24 ¹	Other	N/A	2	1500	4.4	270°	1.923
May 24 ²	Raster	N/A	2	2050	4.8	272°	1.907
May 25	Box	1	2	1800	9.0	217°	1.920
May 28	Box	2	3	1400	7.1	322°	1.897
May 29	Box	2	2	1000	4.6	195°	1.899
June 3	Raster	N/A	1	1250	2.7	149°	1.898

Table 4: Optimized natural gas emission rates for each flight as well as corrected emission rates adjusting for errors in the model wind speed and boundary layer height. For wind speed and boundary layer height error, a negative value represents a model value less than the observations.

Day	Optimized NG Emission Rate (% of production)	Wind Speed Error (6)	Boundary Layer Height Error (7)	Corrected NG Emission Rate (% of production)
May 14	0.37	-31%	-33%	0.80
May 21	0.53	3%	39%	0.37
May 22	1.15	37%	-18%	1.02
May 23	0.45	34%	-9%	0.37
May 24	0.68	48%	-21%	0.58
May 24	0.36	48%	-21%	0.30
May 25	0.99	3%	-43%	1.69
May 28	0.33	-4%	-8%	0.37
May 29	0.35	4%	1%	0.33
June 3	0.26	19%	-8%	0.24
Average	0.55	16%	-12%	0.61

Table 5: Emission rates and potential errors associated with the model optimization technique. r-values represent the correlation between the model and observation-derived upstream natural gas enhancements.

Day	Optimized Upstream Emission Rate (% of production)	r-value Model vs Obs NG Sources	Background Error	Non-Upstream Gas Inventory Error	Model Performance Error	Total Error	2 σ Confidence Interval (% of Production)
May 14	0.37	0.20	$\pm 24\%$	$\pm 19\%$	$\pm 17\%$	$\pm 35\%$	± 0.13
May 21	0.53	0.31	$\pm 24\%$	$\pm 13\%$	$\pm 30\%$	$\pm 41\%$	± 0.22
May 22	1.15	0.47	$\pm 38\%$	$\pm 5\%$	$\pm 37\%$	$\pm 53\%$	± 0.61
May 23	0.45	0.10	$\pm 39\%$	$\pm 13\%$	$\pm 42\%$	$\pm 59\%$	± 0.26
May 24 ¹	0.68	0.31	$\pm 24\%$	$\pm 81\%$	$\pm 17\%$	$\pm 86\%$	± 0.58
May 24 ²	0.36	0.11	$\pm 51\%$	$\pm 150\%$	$\pm 31\%$	$\pm 161\%$	± 0.57
May 25	0.99	0.43	$\pm 29\%$	$\pm 15\%$	$\pm 30\%$	$\pm 44\%$	± 0.44
May 28	0.33	0.33	$\pm 76\%$	$\pm 12\%$	$\pm 20\%$	$\pm 79\%$	± 0.26
May 29	0.35	0.58	$\pm 24\%$	$\pm 11\%$	$\pm 19\%$	$\pm 33\%$	± 0.12
June 3	0.26	0.37	$\pm 31\%$	$\pm 12\%$	$\pm 24\%$	$\pm 41\%$	± 0.11

Table 6: Emission rates from mass balance calculations on applicable days, with emission ranges associated with a ± 5 ppb error in the background value.

Flight	CH ₄ Production within box (Gg hr ⁻¹)	Mass Balance CH ₄ Flux (kg hr ⁻¹)	Non-Upstream CH ₄ Emissions (kg hr ⁻¹)	Calculated Upstream Emission Rate (% of production)	2 σ Confidence Interval (% of Production)
May 22 ₁	4.96	53800	2250	1.04	± 1.09
May 22 ₂	4.96	27400	2250	0.51	± 1.08
May 23 ₁	4.05	5600	934	0.11	± 0.07
May 23 ₂	4.05	5500	934	0.11	± 0.07
May 28 ₁	3.73	7100	706	0.17	± 0.11
May 28 ₂	3.73	6000	843	0.14	± 0.10
May 29 ₁	4.63	27900	1622	0.57	± 0.30

Table 7: Relative error associated with the different sources of uncertainty in the aircraft mass balance.

Flight	Wind Speed Error	Background Error	ABL Error	Inventory Error	Total Error (1σ)	Upstream Emission Rate (% of Production) w/ 2σ Confidence Interval
May 22 ₁	±3%	±56%	±9%	±5%	±57%	1.04 ±1.09
May 22 ₂	±3%	±121%	±9%	±8%	±121%	0.51 ±1.08
May 23 ₁	±3%	±24%	±7%	±20%	±32%	0.11 ±0.07
May 23 ₂	±3%	±26%	±7%	±21%	±34%	0.11 ±0.07
May 28 ₁	±3%	±31%	±7%	±11%	±34%	0.17 ±0.11
May 28 ₂	±3%	±33%	±7%	±16%	±38%	0.14 ±0.10
May 29 ₁	±3%	±28%	±20%	±8%	±36%	0.57 ±0.30

Table 8: Production statistics from mid-2014 for various shales across the United States (Hughes 2014).

	Barnett	Fayetteville	Haynesville	Marcellus	Bradford/ Susquehanna County, PA
# of Producing Wells	16100	4500	3100	7000	1558
Total Production (Bcf day ⁻¹)	5.0	2.8	4.5	12	5.01
Production per well (MMcf day ⁻¹)	0.31	0.56	1.25	1.71	3.22

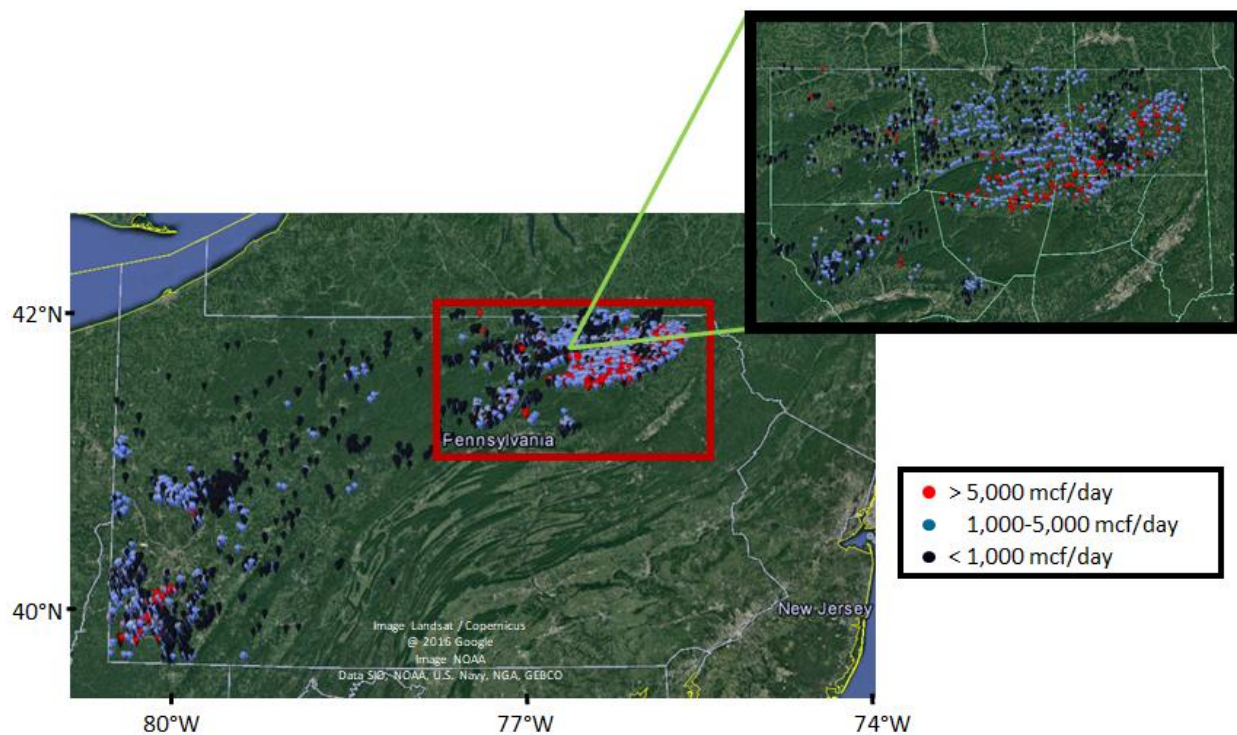


Figure 1: A map of the unconventional wells in Pennsylvania dotted in purple. Production values of wells for May 2015 are indicated by the marker colour. Red rectangle and zoom-in show the region of focus for this study, 41.1-42.2°N 75.2-77.6°W.

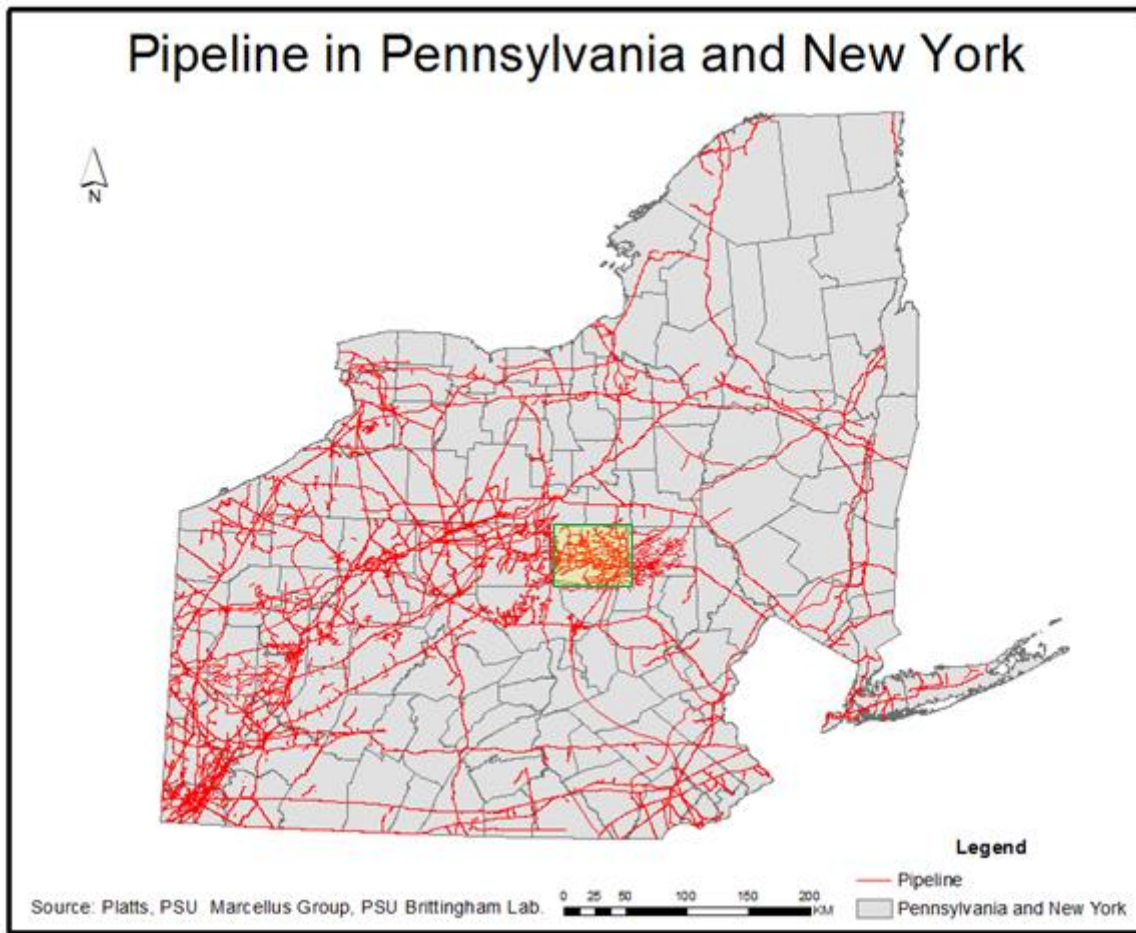


Figure 2: A map of transmission and gathering pipelines for the state of PA and NY. Transmission pipelines are provided by Platts Natural Gas Pipelines product. Gathering pipelines associated with unconventional wells in PA are extrapolated using information on existing gathering pipelines provided by Bradford County, PA (highlighted in yellow).

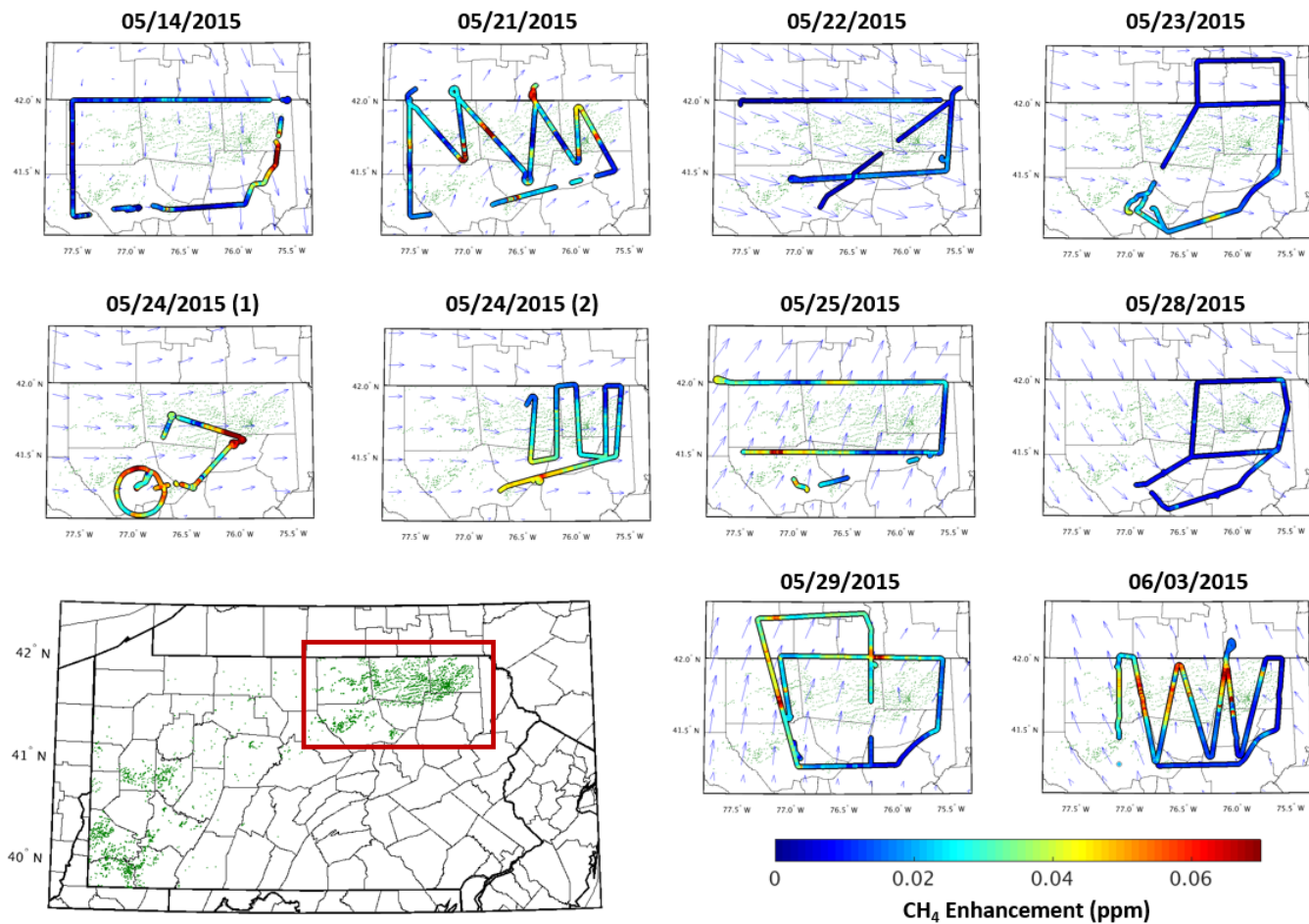


Figure 3: Observed CH₄ enhancements within the boundary layer from each of the 10 afternoon flights used in this study, with green dots showing the location of unconventional wells in PA and blue arrows showing the modelled wind direction during the time of the flight. CH₄ enhancements are calculated by taking the observed CH₄ mole fraction values and subtracting off the flight's background CH₄ value shown in Table 3.

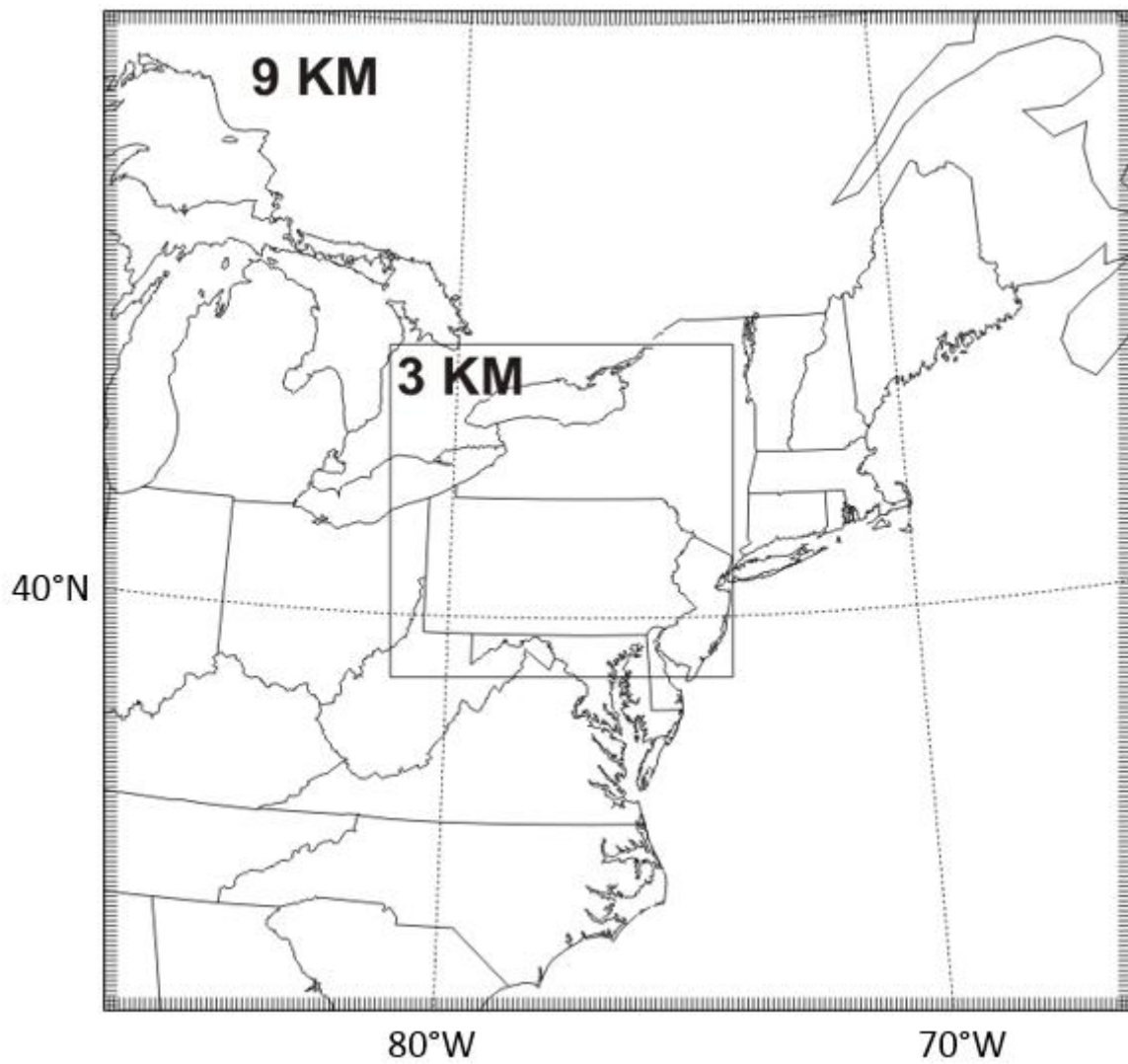


Figure 4: Model domain and resolutions used within the transport model. All emissions used for this study are contained within the 3 km resolution domain.

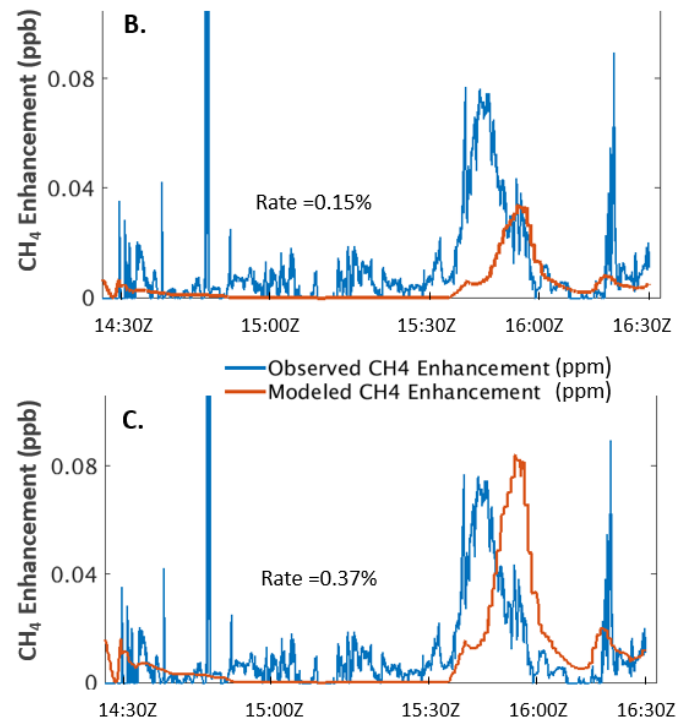
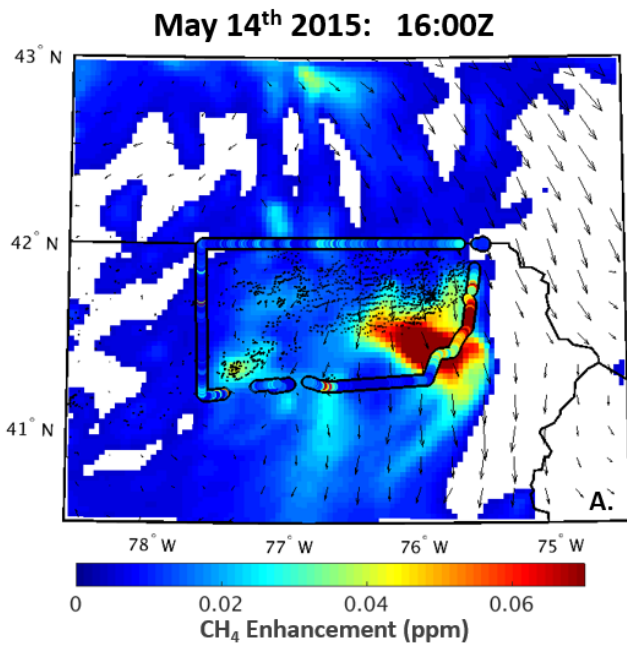


Figure 5: (a.) Observed vs model projected CH₄ enhancements during the May 14th, 2015 at 16Z. (b.) Comparison of observed natural gas enhancement to modelled natural gas enhancement along flight path, with upstream emission rate optimized by minimizing the absolute error between the datasets. (c.) Same as previous, but optimized by minimizing the sum of the error between the datasets.

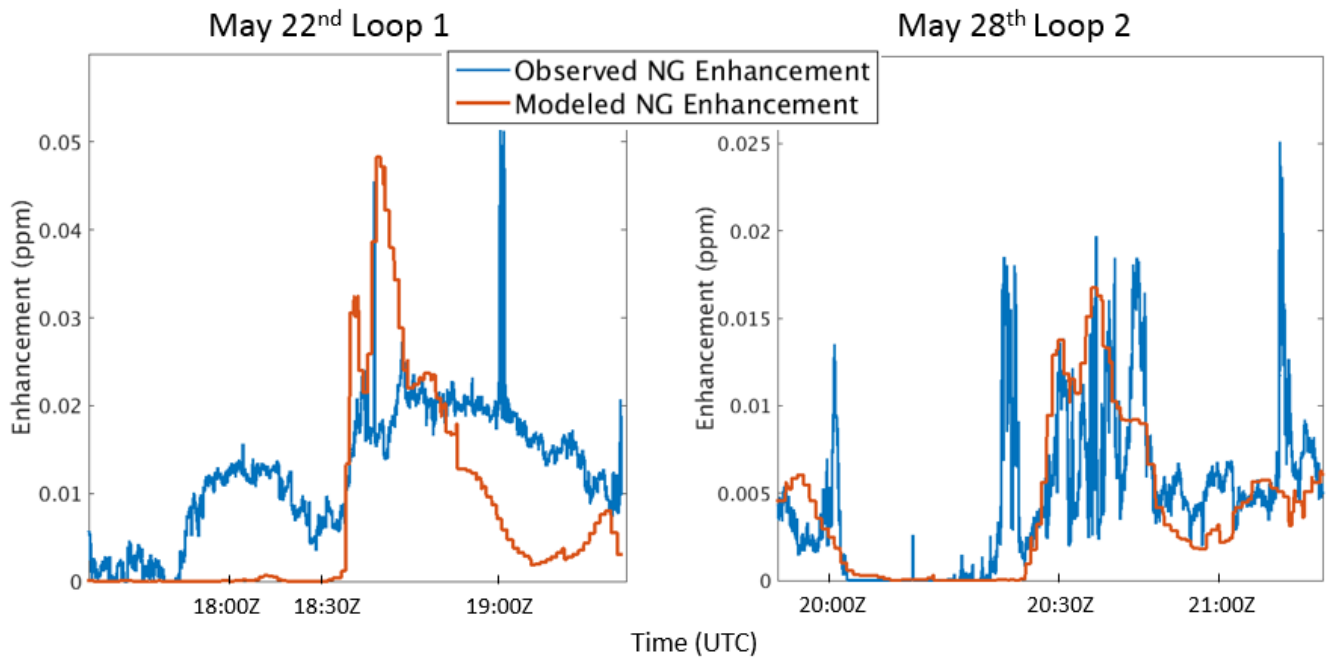


Figure 6: Comparison of observed natural gas enhancement to modelled natural gas enhancement for segments along the (left) May 22nd flight and (right) May 28th flight. A distinct lack of representativeness of the observations in the modelled enhancement can be seen in the May 22nd flight compared to the May 28th flight.

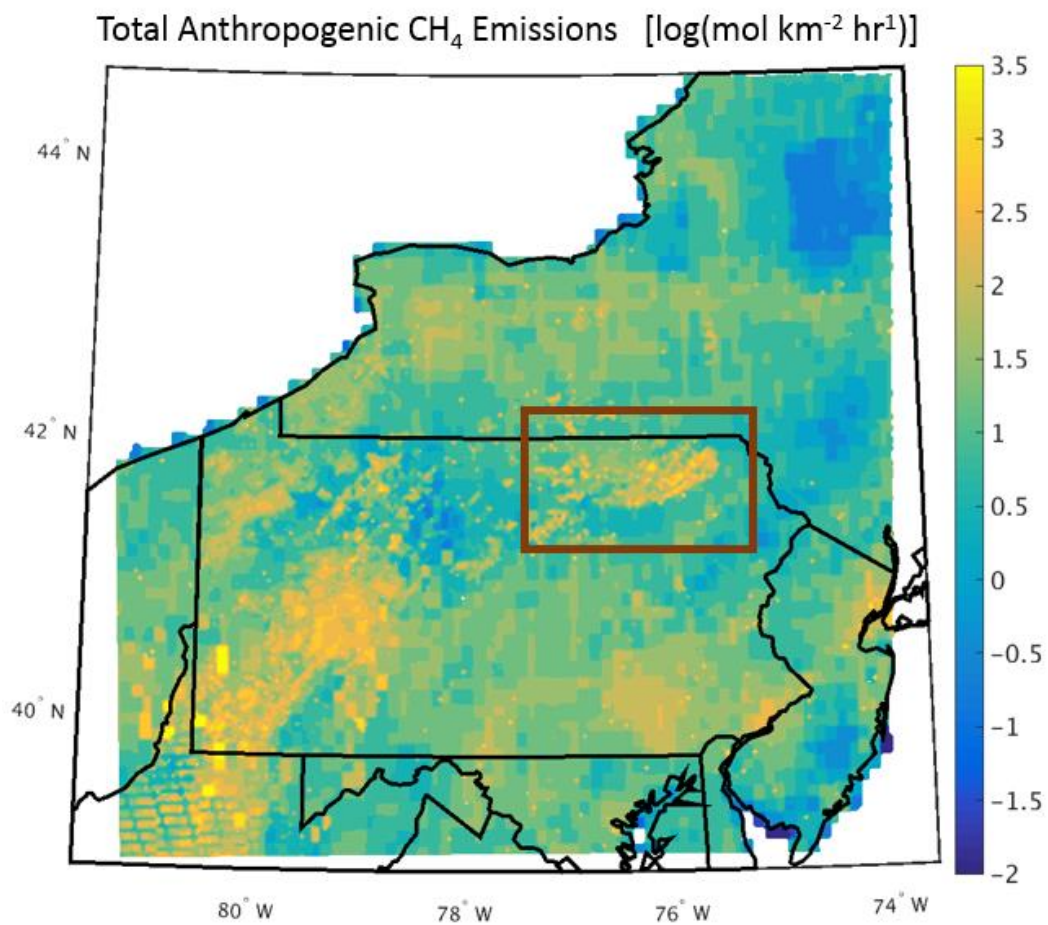


Figure 7: A log scale contour of the anthropogenic CH₄ emissions inventory from this study used within the transport model. The red rectangle surrounds the study region where the aircraft campaign took place.

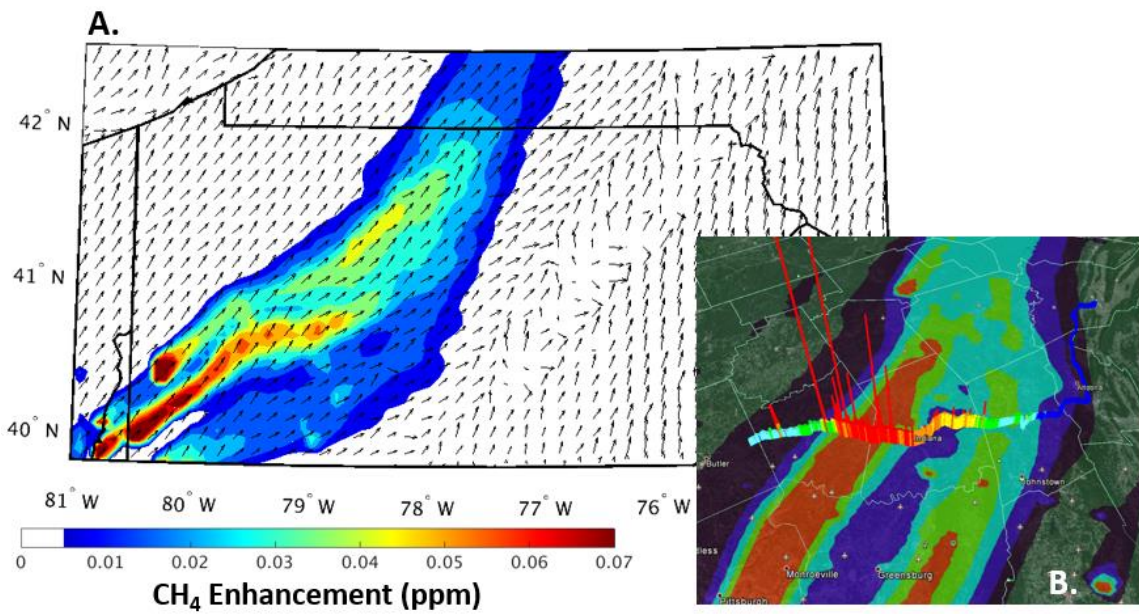


Figure 8: (a.) Model projected CH₄ enhancement at the surface associated with underground, surface, and abandoned coal mines on May 27th, 2015 at 19Z, with the shaded regions showing the CH₄ enhancement and the arrows representing the wind direction. (b.) Projected enhancement from a. mapped over measured CH₄ enhancement from a driving campaign. The height and colour of the bars represents the scale of the CH₄ enhancement.

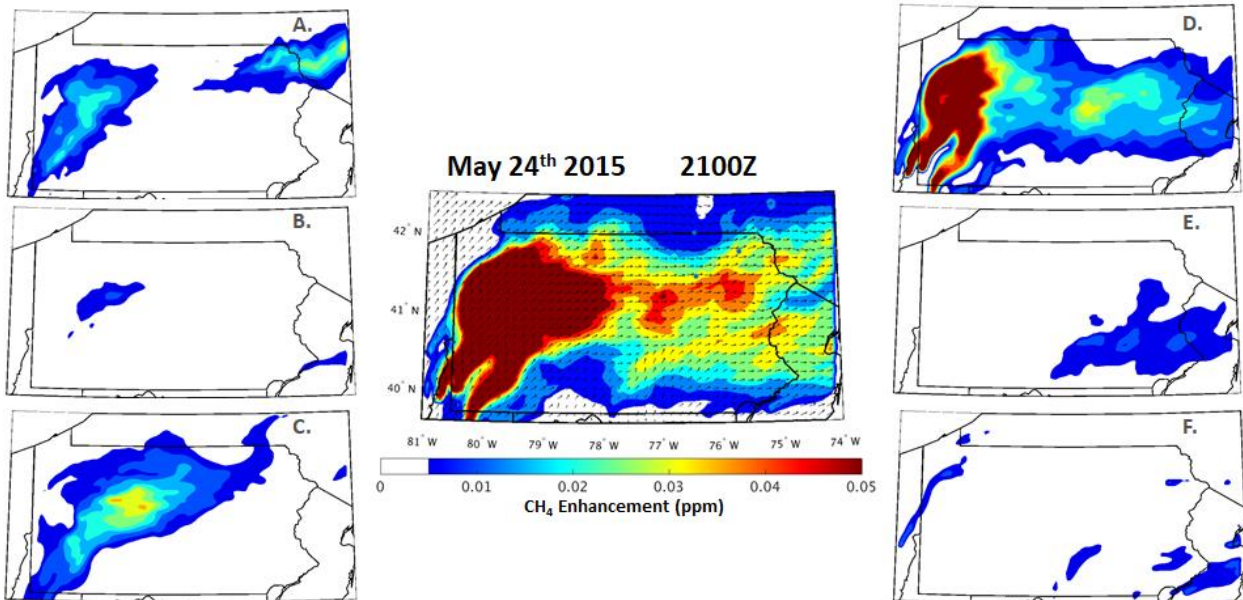


Figure 9: Projected CH₄ enhancements during the late afternoon flight of May 24th, 2015 at 2100Z, 700m above ground level from (A) upstream unconventional gas processes (B) downstream unconventional gas processes (C) conventional production (D) coal mines (E) animal emissions and (F) landfills and other sources within the EPA GHG Inventory Report. The centre figure is a map of the combined enhancement from sources A-F.

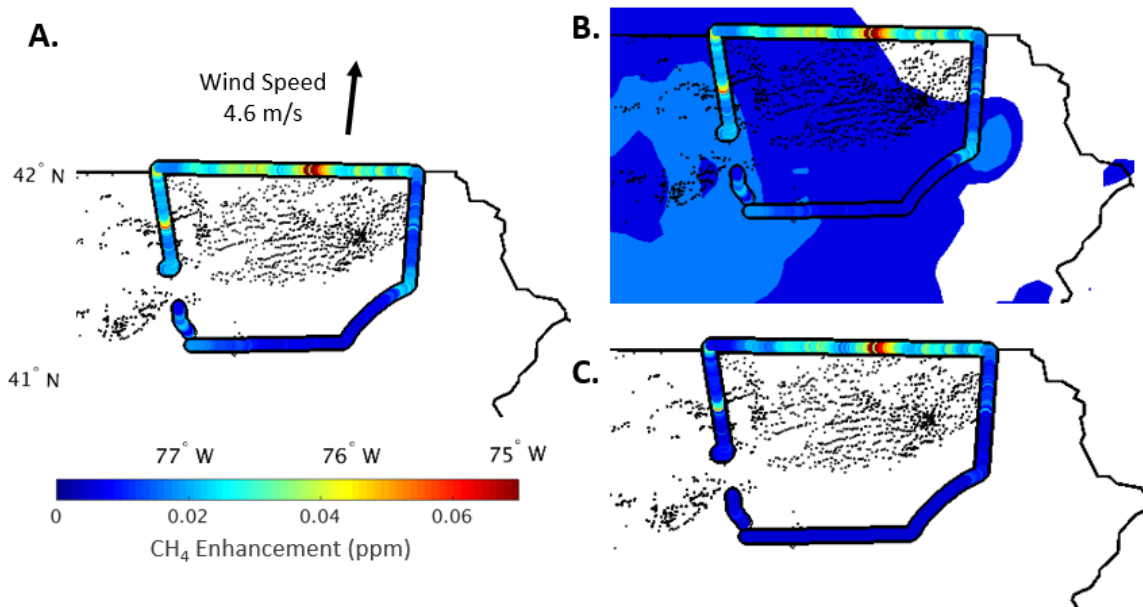


Figure 10: (a.) Observed CH_4 enhancements from within the boundary layer during the first loop of the May 29th aircraft campaign. (b.) Aircraft observations laid overtop modelled CH_4 concentrations at 700 m from sources unrelated to emissions from upstream gas production. (c.) Observed CH_4 enhancements from the May 29th flight after subtracting off modelled sources in b. The new set of observations represent the observation-derived upstream gas enhancement during the flight.

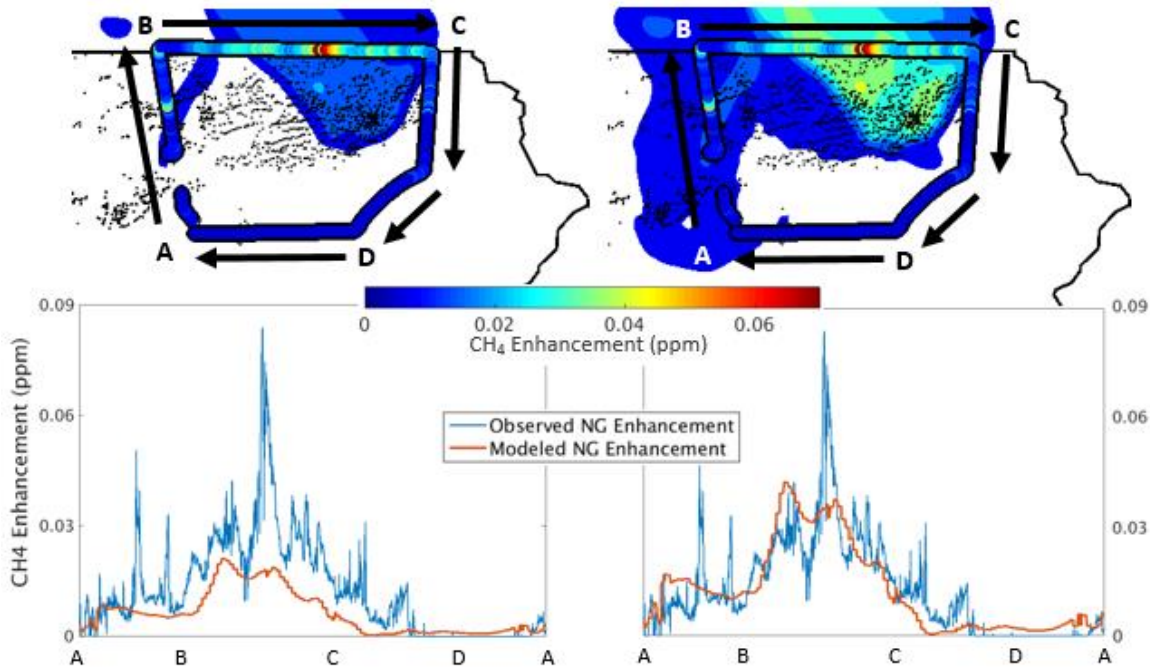


Figure 11: (top-left) Observed enhancement from unconventional natural gas production ovetop projected upstream natural gas enhancements at 700 m from the first loop of the May 29th flight, using an upstream gas emission rate of 0.13% of production. (bottom-left) Direct comparison of the observed natural gas enhancement vs. the modelled enhancement following the path from A-D using an unconventional emission rate of 0.13%. (top-right, bottom-right). Same as left figures, except using the optimized upstream emission rate of 0.26%

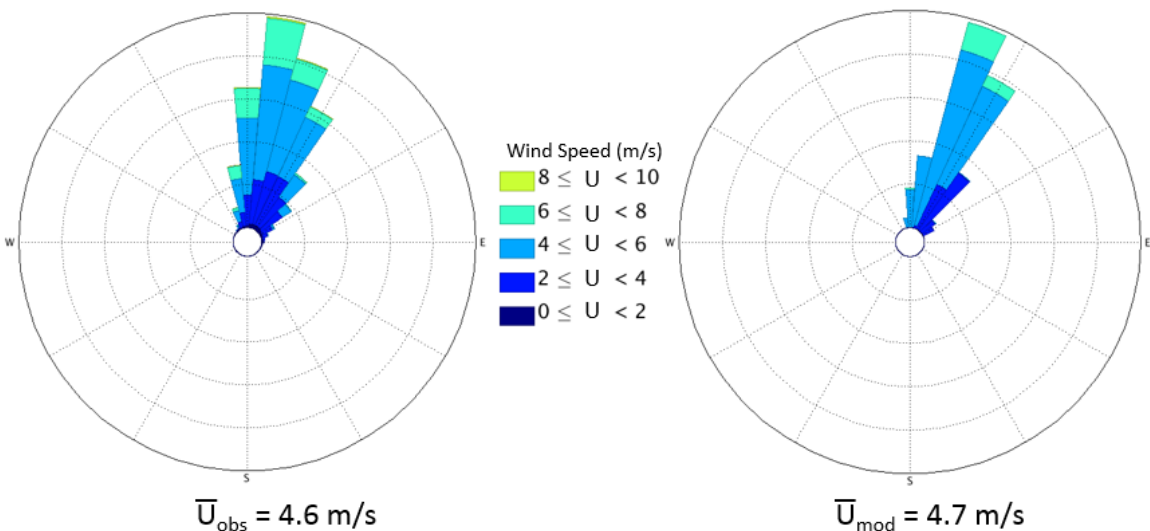


Figure 12: Wind rose of aircraft observations (left) within the boundary from the first loop of the May 29th flight compared to modelled winds following the flight path (right).

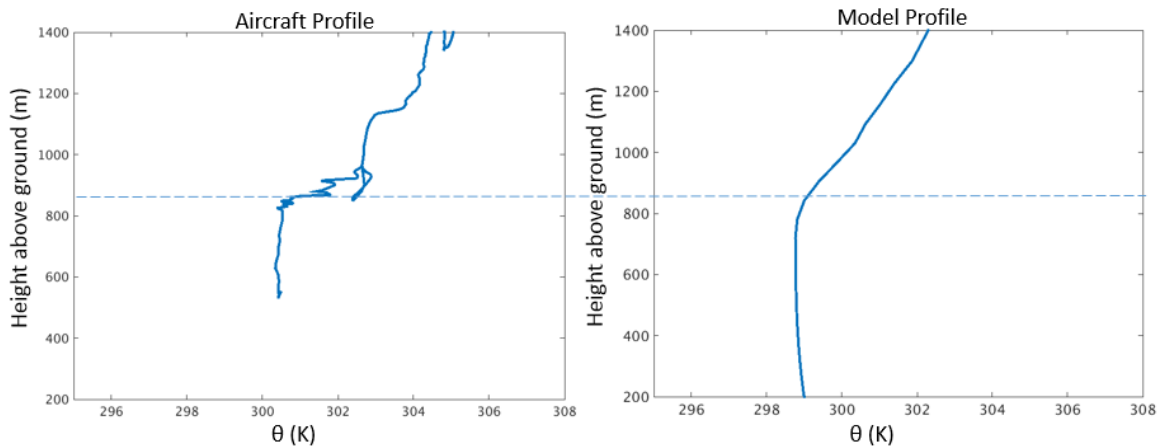


Figure 13: (left) Observed potential temperature profile with height from the first aircraft spiral on the May 29th flight at 17Z. (right) Modelled potential temperature at the location and time at which the aircraft spiral occurred. In both cases, an inversion in the potential temperature profile begins to occur around 850m.

May 24th 2015: Late-Afternoon Flight

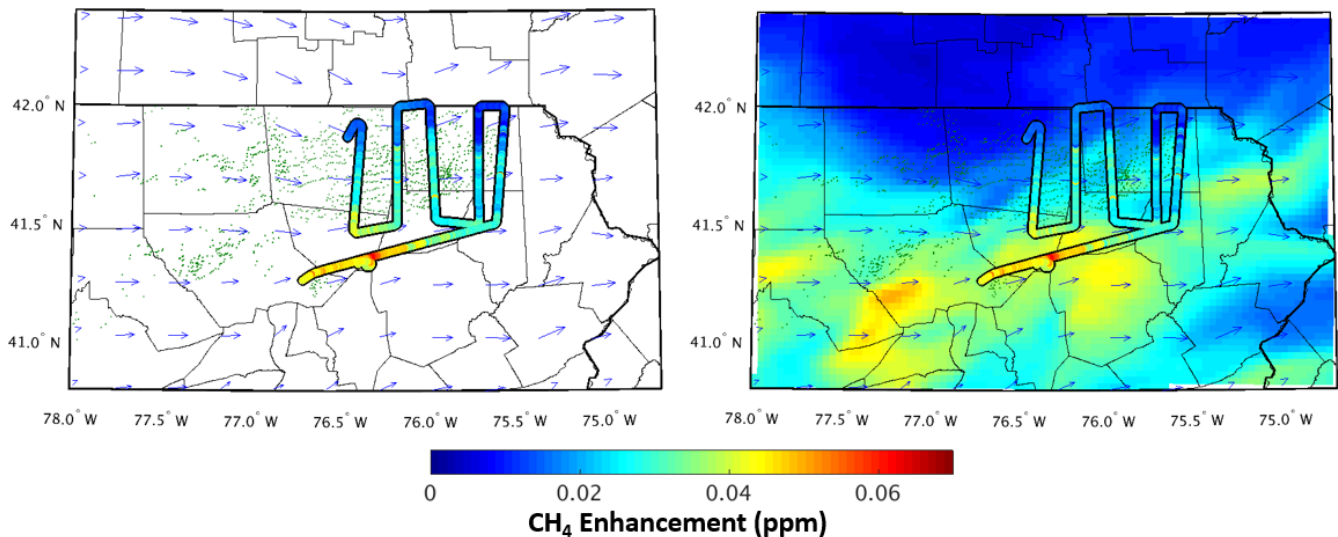


Figure 14: (left) Observed CH₄ enhancement from the late-afternoon flight on May 24th, 2015. (right) Observed CH₄ enhancement compared to the model projected CH₄ enhancement from the sum of all sources in the region. The colour scale of observed and projected enhancements is scaled 1:1, with matching colours indicating matching values. Modelled wind vectors and CH₄ concentrations are from 700 m model height level.

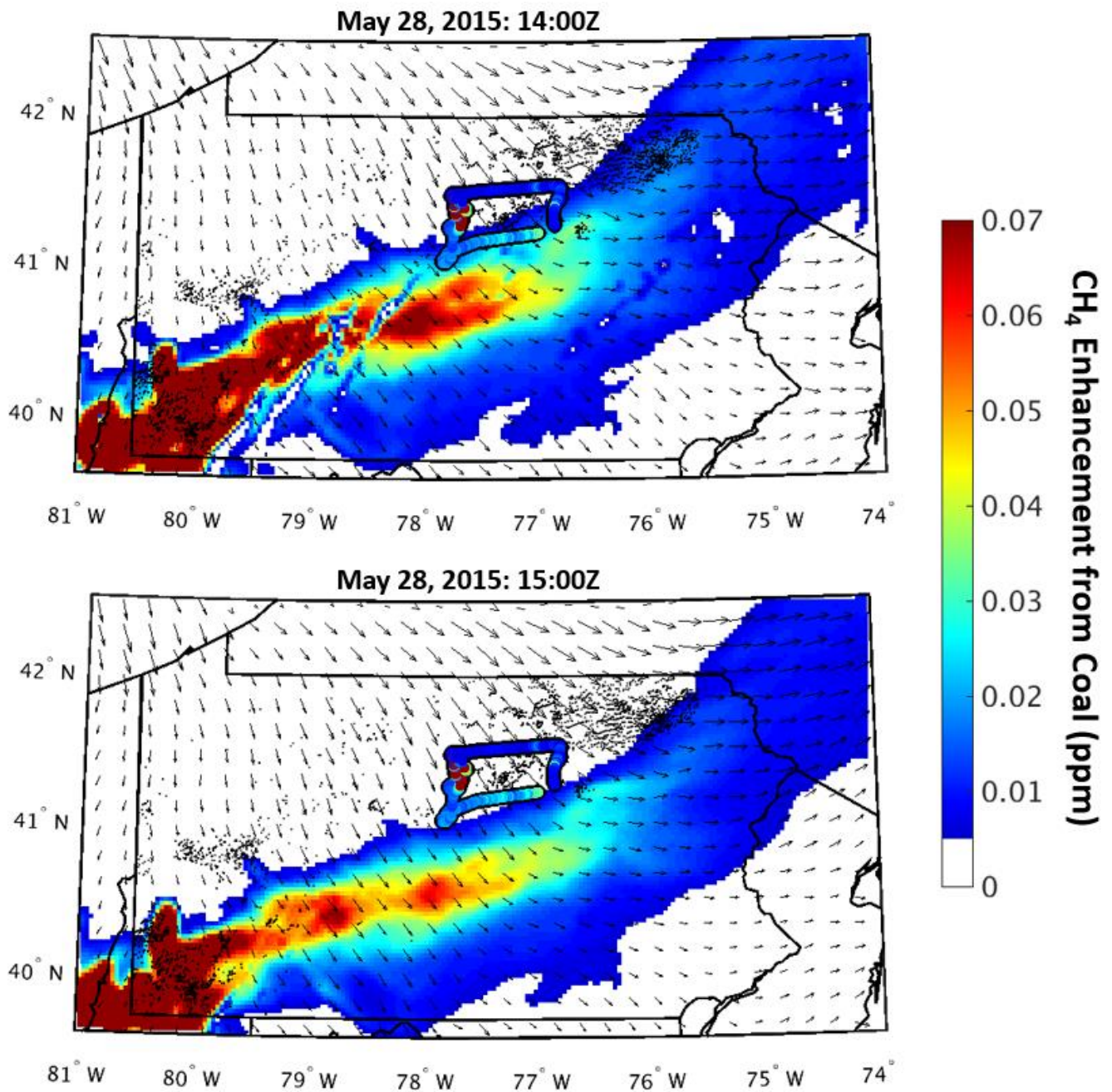
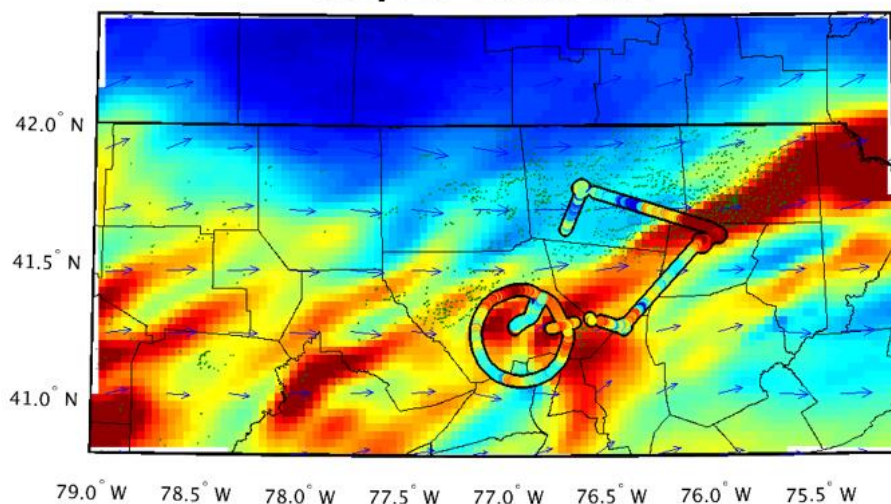
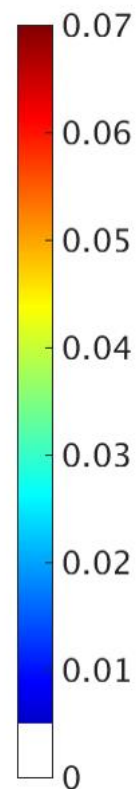
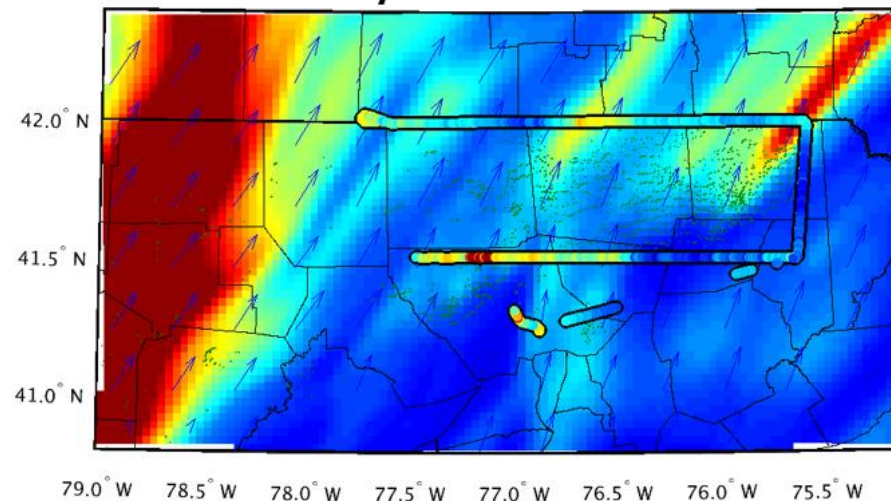


Figure 15: Observed CH₄ enhancements from an early flight on May 28th, 2015 compared to projected CH₄ enhancements from coal emissions modelled at (top) 14:00Z and (bottom) 15:00Z. The one hour time difference results in vastly different projected enhancements across the southern portion of observations. Modelled wind vectors and CH₄ concentrations are from the 700 m model height level.

May 24th 2015: 17Z



May 25th 2015: 19Z



CH₄ Enhancement (ppm)

Figure 16: Observed vs model projected CH₄ enhancements during (top) the early afternoon flight of May 24th, 2015 at 17Z and (bottom) the flight of May 25th, 2016 at 19Z. Modelled wind vectors and CH₄ concentrations are from 700 m model height level.

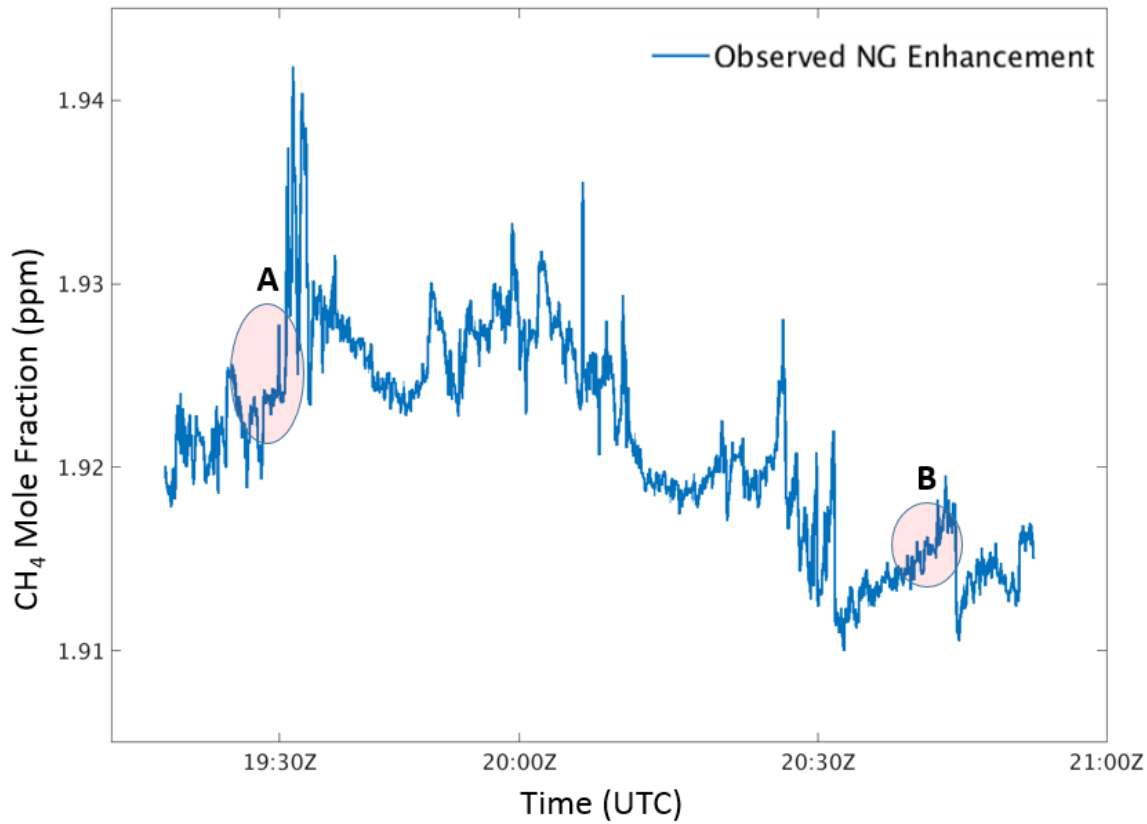


Figure 17: Time series of CH₄ mole fractions from the second loop of the May 22nd flight. Observations at the shaded areas below A and B were taken at similar locations in space, showing the change in the background mole fraction across time.

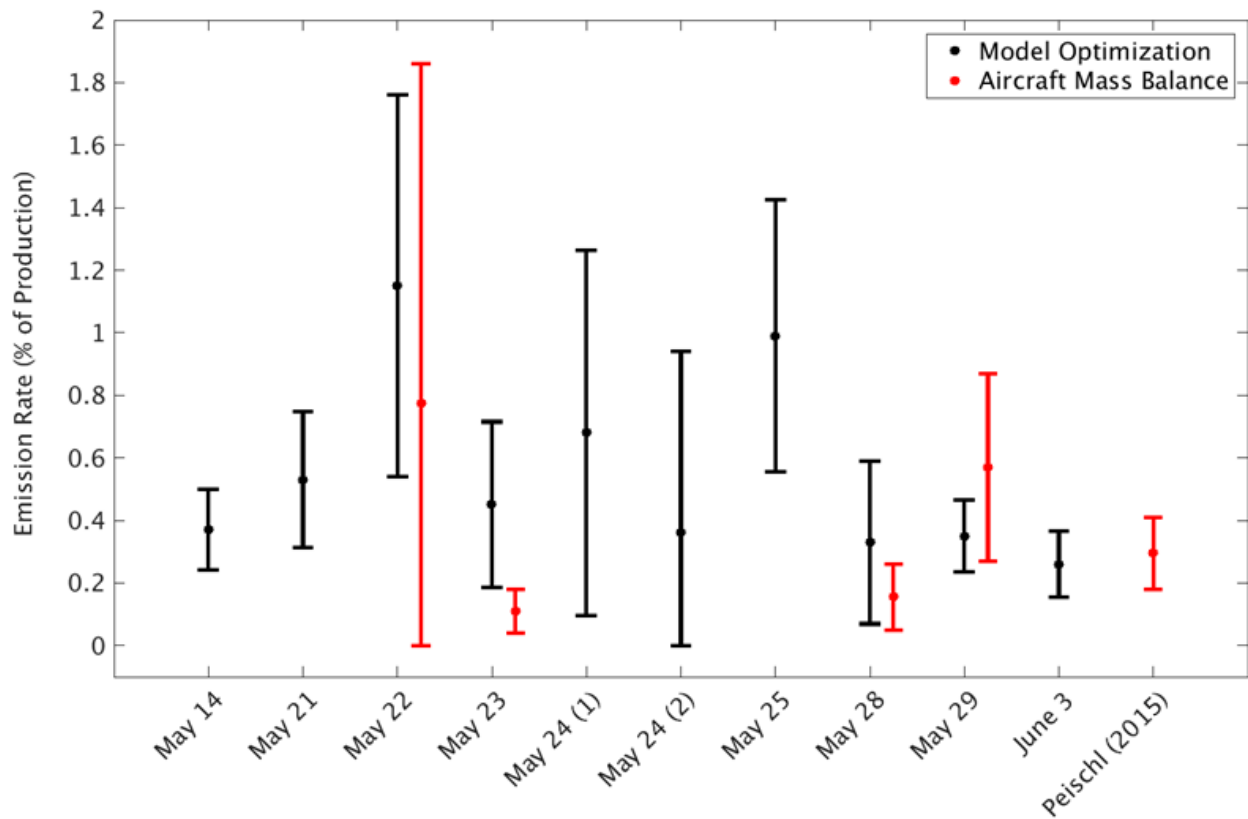


Figure 18: Calculated upstream natural gas emission rates using (black) model optimization technique and (red) aircraft mass balance technique. Error bars represent the 2σ confidence interval for each flight. Mass balance performed in Peischl et al (2015) included for comparison.

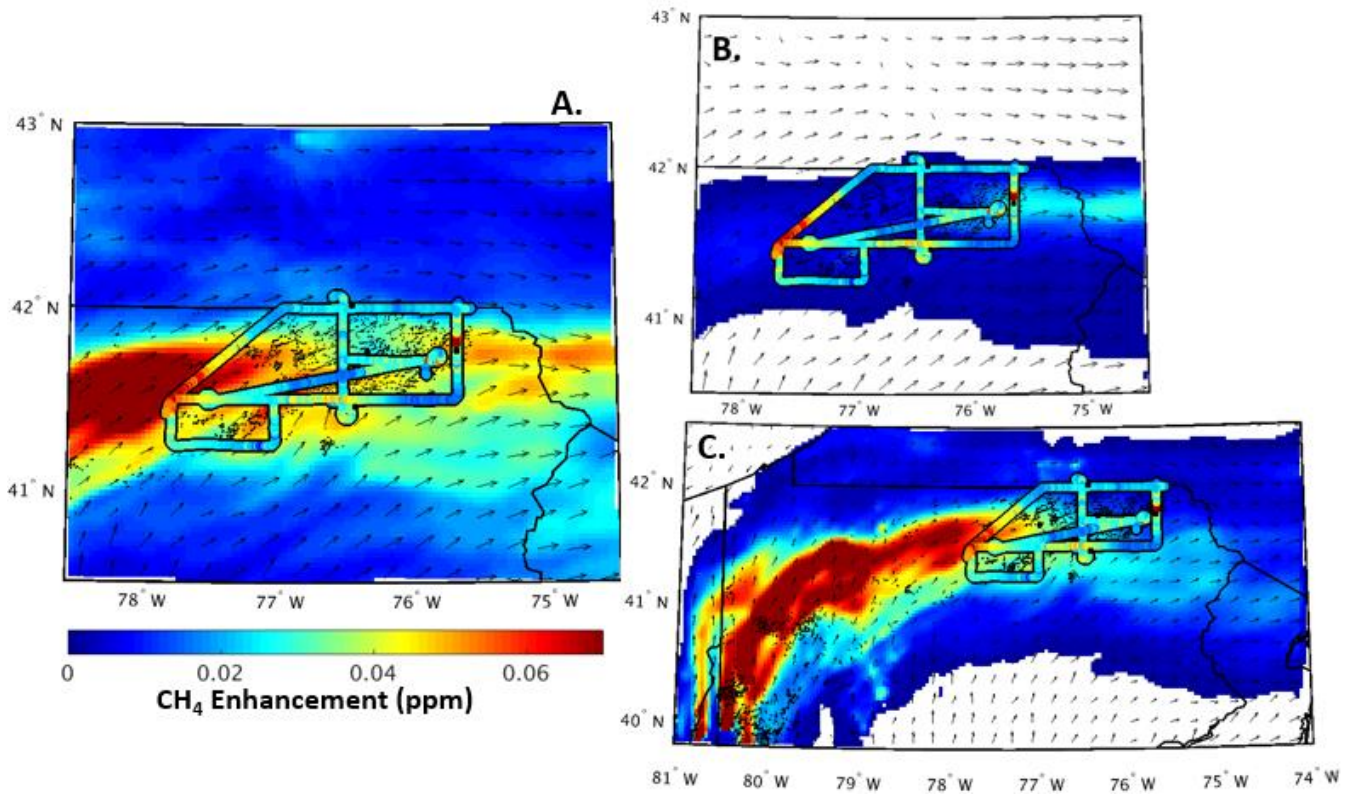


Figure 19: Observations vs modelled enhancements of the flight from Peischl et. al (2015) for July 6th, 2013. (a.) Observed enhancements from the flight over model projected enhancements from all sources at 21Z. (b.) Projected enhancement from upstream gas processes using a 0.4% emission rate. (c.) Projected enhancement from coal sources in southwestern PA. Modelled wind vectors and CH₄ concentrations are from 700 m model height level.